EPSC Abstracts
Vol. 10, EPSC2015-25, 2015
European Planetary Science Congress 2015

Space weathering of asteroids as observable with GAIA

Z. Kanuchova (1,2), R. Brunetto (3), D. Fulvio (4), G. Strazzulla (2)
(1) Astronomical Institute of Slovak Academy of Sciences, SK-05960 T. Lomnica, Slovakia
(2) INAF-Osservatorio Astrofisico di Catania, Via S. Sofia 78, I-95123 Catania, Italy
(3) Institut d'Astrophysique Spatiale (IAS), Université Paris-Sud, UMR 8617 - CNRS INSU, Bât 121, F-91405 Orsay, France
(4) Departamento de Física, Pontifícia Universidade Católica do Rio de Janeiro, Rua Marquês de São Vicente 225, 22451-900, Rio de Janeiro, RJ, Brazil

Abstract

Among the scientific objectives of the GAIA mission, there is great scientific interest in detecting asteroids and comets in our Solar System. In the next years, GAIA is expected to strongly contribute to this search because of its unprecedented sensitivity to faint, moving objects. We investigate how to use the spectrophotometric data of asteroids that GAIA is in the process of acquiring (scientific mission started in summer 2014 for 5 years) to evidence space weathering processes.

Along with asteroid spectral reflectivities, one of the products are the Spectra Shape Coefficients, a sort of colours obtained by integrating the spectra in predefined bands.

To this end we have checked which colours, among those chosen by the GAIA team as wavelengths for the spectral shape coefficients, can be more useful to evidence the spectral alteration induced by space weathering as simulated in the laboratory by irradiation with energetic ions and pulsed lasers.

We show that a diagram plotting the colour index SSC_{530}-SSC_{953} vs the SSC_{752}-SSC_{953} one, well defines a region where the GAIA observations of S-type asteroids and Vestoids can evidence the space weathering experienced by the observed objects.

1. Introduction

The surfaces of atmosphere-less bodies are irradiated by a large variety (in terms of energy and mass) of cosmic and solar wind ions, by UV photons, and collide with interplanetary dust. These effects are globally known as "space weathering" and have been evidenced on several asteroid types on the basis of laboratory studies on terrestrial silicates and meteorites (for a recent review see [1]).

An enormous advance in the understanding of asteroid space weathering may come from the Gaia mission (ESA) that is surveying the entire sky and it is expected to observe about 400,000 asteroids, for which high precision astrometry and photometry will be obtained [2]. It has been estimated that a spectral characterization will be obtained for at least 100,000 asteroids from the low-resolution spectra (0.35-0.95 μm) obtained by Gaia [3].

Here we discuss how to use the spectrophotometric data of GAIA to evidence space weathering of S-type asteroids and Vestoids. Our investigation is based on many experimental data we have collected in the laboratory after ion bombardment of terrestrial silicates and meteorites [4, 5] or pulsed laser irradiation [6] or even from RELAB database [7]. We show that GAIA observations may be used to provide a deeper and statistically stronger view of asteroid weathering.

2. Spectral analysis

The GAIA spectrophotometers are based on two low-resolution prisms, one (BP) is optimized for the "blue" wavelengths (330–680 nm) and one (RP) for the "red" wavelengths (640–1000 nm).

Eight spectral shape coefficients (SSC) have been suggested to characterize at the best the spectral response of the two filters. These SSCs are peaked at 380, 467, 530, 639, 668, 752, 824 and 953 nm (see Figure 7 in [3]). We have measured the reflectivity of our laboratory samples at these wavelengths before and after energetic processing, to find the best colour indexes that evidence the effect of the processing. As an example we show the spectra of a bulk sample of the meteorite Kosice before and after ion irradiation (Fig. 1). Also indicated in the figure are the positions of the three wavelengths (corresponding to the

wavelengths of three of the SSCs listed above) that we use to determine the two color indexes found to best represent the effects of space weathering. These indexes are SSC530-SSC952 and SSC752-SSC952.

The two color indexes measured for several samples of silicates and meteorites irradiated by energetic ions or laser pulses are plotted one vs. the other in Fig. 2. It is evident from the figure that there is a trend for all samples to exhibit color indexes that increase because of the energetic processing. The increase in the SSC_{530}-SSC_{952} color index testifies for the reddening of the sample [5], the increase of the SSC_{752}-SSC_{952} one reflects the monotonic decreases of the 1 μm band with ion bombardment [4].

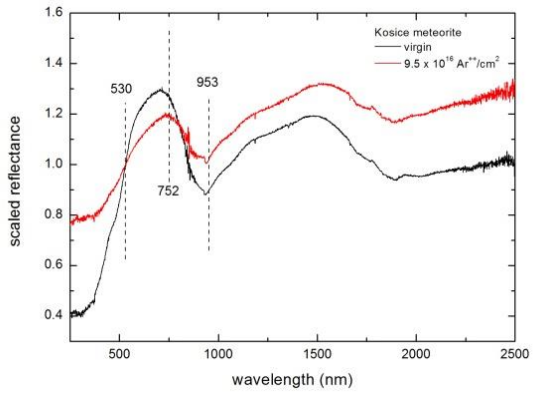

Figure 1: Scaled (to 530 nm) reflectance spectra of a bulk sample of the meteorite Kosice before and after ion irradiation.

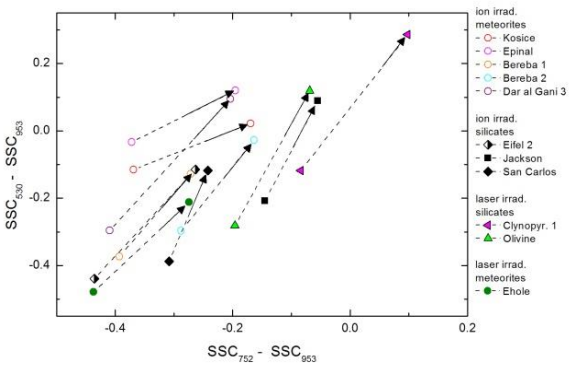

Figure 2: The colour index SSC_{530}-SSC_{952} is plotted vs the SSC_{752}-SSC_{952} one. The data refer to samples of silicates and meteorites irradiated by energetic ions or laser pulses (arrows indicate the increasing dose).

Conclusion

In this work, we discuss how the data provided by the GAIA mission may be used to evidence space weathering of S-type asteroids and Vestoids. Our investigation is based experimental data we have collected in the laboratory after ion bombardment of terrestrial silicates and meteorites, pulsed laser irradiation, or even from RELAB database.

We show that GAIA observations may be useful to provide a deeper and statistically stronger understanding of asteroid space weathering.

Acknowledgements

The research of Z.K. has been supported by VEGA - The Slovak Agency for Science, Grant No. 2/0032/14.

References

[1] Brunetto, R., et al. 2015, Asteroid Surface Alteration by Space Weathering Processes. Asteroids IV, in press.

[2] Cellino, A., Dell´Oro, A. 2012, The derivation of asteroid physical properties from Gaia observations. Planet. Space Sci. 73, 52-55

[3] Delbo, M. et al. 2013, Asteroid spectroscopy with Gaia. Planet. Space Sci. 73, 86-93

[4] Strazzulla, G. et al. 2005, Spectral alteration of the Meteorite Epinal (H5) induced by heavy ion irradiation: a simulation of space weathering effects on near-Earth asteroids. Icarus 174, 31-35

[5] Fulvio, D., et al. 2012, Space weathering of Vesta and V-type asteroids: new irradiation experiments on HED meteorites. Astron. Astrophys. 537, L11

[6] Brunetto, R., et al. 2006, Space weathering of silicates simulated by nanosecond pulse UV excimer laser. Icarus 180, 546-554

[7] Pieters, C. M., Hiroi, T. 2004, RELAB (Reflectance Experiment Laboratory): A NASA Multiuser Spectroscopy Facility. In: 35th Lunar and Planetary Science Conference, March 15-19, 2004, League City, Texas, abstract no.1720

EPSC Abstracts
Vol. 10, EPSC2015-30, 2015
European Planetary Science Congress 2015

Fossilized condensation lines in the Solar System proto-planetary disk

A. Morbidelli (1), B. Bitsch (2), A. Crida (1), M. Gounelle (3), A. Johansen(2), E. Lega (1);
(1) Observatoire de la Cote d'Azur, Nice France (2) Univ. of Lund, Sweden (3) Museum National d'Histoire Naturelle, Paris, France (morby@oca.eu)

Abstract

A proto-planetary disk cools very quickly, so that the snowline is expected to move inwards of 2 AU within a My. However, ordinary chondrites, which formed presumably in the asteroid belt at about 3 My, contain very little water and show little signs of water alteration. In this talk we propose a scenario that explains why the chemistry of the objects of the solar system reflects the position of the snowline fossilized at the time the proto-Jupiter achieved a mass of the order of 20 Earth masses.

EPSC Abstracts
Vol. 10, EPSC2015-36, 2015
European Planetary Science Congress 2015

UV bluing after Space Weathering of silicates and meteorites

Z. Kanuchova (1,2), R. Brunetto (3), D. Fulvio (4), G. Strazzulla (2)
(1) Astronomical Institute of Slovak Academy of Sciences, SK-05960 T. Lomnica, Slovakia
(2) INAF-Osservatorio Astrofisico di Catania, Via S. Sofia 78, I-95123 Catania, Italy
(3) Institut d'Astrophysique Spatiale (IAS), Université Paris-Sud, UMR 8617 - CNRS INSU, Bât 121, F-91405 Orsay, France
(4) Departamento de Física, Pontifícia Universidade Católica do Rio de Janeiro, Rua Marquês de São Vicente 225, 22451-900, Rio de Janeiro, RJ, Brazil

Abstract

Asteroid surface space weathering has been investigated both observationally and experimentally, mostly focusing on the effects on the visible-near infrared (VNIR, 0.4-2.5 μm) spectral range. Here we present laboratory near-UV (NUV, 200-400 nm) reflectance spectra of ion irradiated (30-400 keV) silicates and meteorites as a simulation of solar wind ion irradiation. These results show that the induced alteration can reproduce the spread observed in the VNIR vs. NUV slope diagram for S-type asteroids. We expect the evidence of weathering processes in the NUV part of spectra before these effects becomes observable at the longer wavelengths [1].

1. Introduction

Asteroid surfaces are continuously altered by solar and cosmic ion irradiation, and micrometeorites. These processes are known as "space weathering". As a consequence of the chemical-physical alterations induced by space weathering, optical properties of asteroid surfaces may change, thus affecting the interpretation of their spectral properties and the efforts to establishing a solid meteorites-asteroids link (e.g., [2], [3]). Direct evidence of the effect of space weathering has been recently provided by the laboratory analyses of particles returned from asteroid 25143 Itokawa by the Hayabusa mission [4].

A number of experimental studies have focused on the spectral alteration induced by irradiating OC meteorites and terrestrial silicates. The results of ion and laser irradiation experiments are, besides other applications, used to estimate timescale for which spectral alterations observed in laboratory may occur in the space environment. As UV bluing occurs with a lower amount of weathering than the VIS-NIR reddening [5], [6], the study of space weathering processes in this spectral region is very actual.

2. Experiments

Samples of different materials – meteorites and terrestrial silicates – have been irradiated with different ions at room temperature, inside a stainless steel vacuum chamber ($P<10^{-7}$mbar) faced to different spectrometers (see e.g., [7], [8]). Spectra of samples were obtained in- and ex-situ after irradiation. We also consider the results obtained after pulsed laser irradiation of silicate samples [9], and meteorites published in the RELAB database [10].

3. Results and discussion

Following the procedure described in [5] we have measured two spectral indexes - the spectral slopes, per nm and computed for the spectra normalized to 0.55 μm - that well represent the colour variations for our samples, before and after irradiation. Results for meteorites are shown in Fig. 1 and compared with those of S-type asteroids and OC meteorites [5]. Also enclosed in Fig. 1 are the data obtained after ns pulsed laser irradiation (from [9] and RELAB [10]).

For some samples we can look at the rate of spectral changes with the increasing of ion fluence or cumulative laser energy. We calculated the first derivative of the NUV and VNIR slopes as functions of ion fluence or laser energy accumulation (Fig.2). We have estimated the astronomical time-scale on an asteroidal surface at a distance of 2.7 AU and exposed to space weathering (Fig.2).

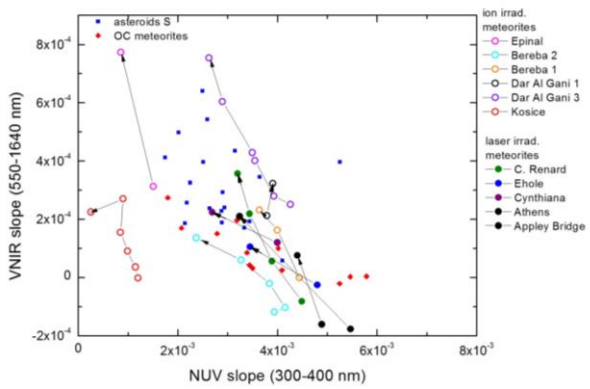

Fig.1: The VNIR spectral index is vs the NUV one.

Laboratory results here presented demonstrate that space weathering of meteorites and terrestrial silicates can reproduce the slope spread shown by S-type asteroids in the VNIR vs NUV slope diagram. This represents a not obvious confirmation of the suggestion by Hendrix and Vilas [5] that was only based on the comparison between the results of observations of asteroids and the laboratory spectra of lunar materials, and indicates the space weathering as the mechanism responsible for the observed spread of slopes.

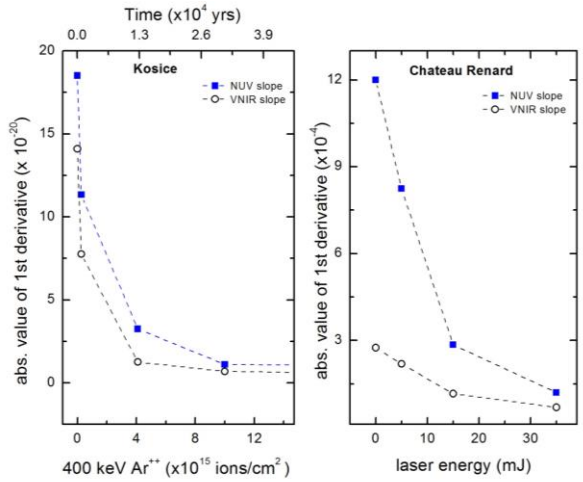

Fig.2: Absolute values of the first derivative of spectral slopes as functions of increasing ion fluence for meteorite Kosice and cumulative laser energy for meteorite Chateau Renard (from RELAB).

For two studied meteorite samples we found the higher rate of changes of NUV spectral slope with respect to the VNIR slopes as the derivative of the NUV spectral slope is always greater than that of the derivative of the VNIR slopes.

We attribute the NUV bluing, analogously to the VNIR reddening, to the formation of iron nanoparticles accompanied by structural modifications (amorphization) of surface silicates.

We expect the evidence of weathering processes in the NUV part of spectra before these effects become observable at longer wavelengths [1], thus searching for the SW effects in the UV range would allow establishing the grade of space weathering for very young asteroidal families.

Acknowledgements

The research of Z.K. has been supported by VEGA - The Slovak Agency for Science, Grant No. 2/0032/14.

References

[1] Kanuchova et al. 2015, Icarus, submitted

[2] Brunetto, R., et al. 2015, Asteroid Surface Alteration by Space Weathering Processes. Asteroids IV, in press.

[3] Hapke, B. 2001. Space weathering from Mercury to the asteroid belt. J. Geoph. Res. 106, 10039 – 10073

[4] Noguchi, T., et al. 2014. Space weathered rims found on the surfaces of the Itokawa dust particles. Meteoritics and Planetary Science 49, 188-214

[5] Hendrix, A.R., Vilas, F., 2006. The effects of space weathering at UV wavelengths: S-class asteroids. Astron. J. 132, 1396 – 1404

[6] Vilas, F., et al. 2015, Searching for the onset of space weathering in S-complex asteroids in the UV. In: 46th Lunar and Planetary Science Conference (2015), Abstact no. 2935

[7] Strazzulla, G. et al. 2005, Spectral alteration of the Meteorite Epinal (H5) induced by heavy ion irradiation. Icarus 174, 31-35

[8] Kanuchova, Z., et al. 2010. Space weathering of asteroidal surfaces. Astron. Astrophys. 517, A60.

[9] Brunetto, R., et al. 2006, Space weathering of silicates simulated by nanosecond pulse UV excimer laser. Icarus 180, 546-554

[10] Pieters, C. M., Hiroi, T. 2004, RELAB (Reflectance Experiment Laboratory): A NASA Multiuser Spectroscopy Facility. In: 35th Lunar and Planetary Science Conference, March 15-19, 2004, League City, Texas, abstract no.1720

EPSC Abstracts
Vol. 10, EPSC2015-57, 2015
European Planetary Science Congress 2015

Recent advances in asteroid polarimetry

A. Cellino (1), E. Ammannito (2,3), S. Bagnulo (4), I.N. Belskaya (5), R. Gil-Hutton (6), P. Tanga (7), E.F. Tedesco (8)
(1) INAF, Osservatorio Astrofisico di Torino, Italy (cellino@oato.inaf.it), (2) INAF, IAPS Roma, Roma, Italy (eleonora.ammannito@iaps.inaf.it), (3) UCLA, Los Angeles, USA, (4) Armagh Observatory, UK (sba@arm.ac.uk), (5) Institute of Astronomy of Kharkiv National University, Ukraine (irina@astron.kharkov.ua) (6) Complejo Astronomico El Leoncito (CASLEO), Argentina (rgilhutton@casleo.gov.ar) (7) Observatoire de la Cöte d'Azur, France (Paolo.Tanga@oca.eu) (8) Planetary Science Institute, USA (eft@psi.edu)

Abstract

Asteroid polarimetry has experienced important advancements in recent years. This includes the discovery of new classes of objects, a new assessment of the relation between geometric albedo and a variety of different polarimetric parameters, the first attempt to use *in situ* analyses of asteroid (4) Vesta to better understand the relation between local surface properties and disk-integrated polarimetric measurements, and the first applications of spectro-polarimetry to the physical characterization of the asteroids. The most recent results in the above topics are briefly summarized.

1. Introduction

Polarimetry is a powerful tool for the physical characterization of atmosphereless solar system bodies. For a long time, however, this technique has been rarely applied in a systematic way to the study of asteroids, due to the difficulty in obtaining several polarimetric measurements per object taken at different epochs, which are needed to successfully exploit the potential of this technique. Moreover, the lack of general physical models of light-scattering phenomena, capable to provide firm and detailed explanations of the variety of polarimetric data exhibited by bodies like the asteroids, has contributed for a long time to discourage many researchers, who considered asteroid polarimetry as a fairly exotic discipline.

The situation has started to change since the 80s and has been rapidly evolving in recent years. New teams of researchers made important efforts to increase the database of asteroid polarimetric data, and to improve our capability to use the results of these measurements as a primary source of information about physical parameters of asteroid surfaces that are very difficult to obtain by means of other techniques. This paper briefly summarizes the situation and presents the most recent advances in the field.

2. Polarimetry as the best technique to derive asteroid albedos

The determination of the geometric albedo is a very important tool for the physical characterization of asteroid surfaces. The geometric albedo, which quantities the reflectance of a planetary surface, is a fundamental parameter, being related to the composition and particle size distribution of the minerals present in the regolith, that is the most external surface layer. The determination of the albedo from polarimetric data is based on some known relations, first tested in laboratory experiments some decades ago, between the geometric albedo and some parameters that describe the polarimetric properties of different materials. In particular, what is observed in asteroid polarimetry is the variation of linear polarization as a function of the phase angle (the latter being the angle between the directions to the Sun and to the observer, as seen from the target body). Polarimetric data obtained at different epochs, corresponding to different phase angles, allow the observers to obtain the so-called phase - polarization curves, which are characterized by a common kind of general morphology, described traditionally by means of a small number of parameters, but with differences that are known to be a function of the albedo.

In the past, different authors have carried out analyses to establish quantitative relations between the parameters describing phase - polarization curves and the geometric albedo. The situation has long been quite confused, since there has never been a convergence to a unique approach, and due to the fact that the calibration of the adopted relations (like the so-called slope - albedo law) has been for a long time a difficult task, limiting the practical application of polarimetric stud-

ies to the derivation of asteroid albedos. As a consequence, most catalogues of asteroid albedos adopted in these years have been obtained by means of other techniques, primarily thermal radiometry.

In a recent paper, [1] have carried out a new extensive analysis of currently available polarimetric data and have proposed updated calibrations of different relations between different polarimetric parameters and the geometric albedo. According to these authors, several reliable relations can be successfully established, and can provide albedo determinations much more accurate than those obtained by means of thermal radiometry.

2.1 The ground truth from Vesta

The asteroid (4) Vesta, visited by the DAWN probe, is an ideal target to better understand the relation between albedo and polarization properties. The reason is that Vesta is the only one asteroid for which a clear variation of linear polarization as a function of rotation has been convincingly proven. After the detailed study of Vesta's surface by the instruments aboard DAWN, it is now possible to carry out analysis aimed at establishing the relation between physical properties of the surface, like albedo, texture and composition, and the disk-integrated polarimetric signal measured from the ground as a function of time, due to the rotation of the asteroid. This exercise has been attempted by [2], who have obtained the first indication about the "ground truth" in asteroid polarimetry.

3. The Barbarians

The discovery of the peculiar polarimetric properties of asteroid (234) Barbara dates back to 2006 [3]. Since then, a small number of other "Barbarian" asteroids have been discovered. Up to a couple of years ago, only a handful of Barbarians were known. The peculiar feature of Barbarians is an unusually large "negative polarization branch", namely an interval of phase angles at which the plane of linear polarization turns out to be parallel to the plane of scattering (the plane containing the Sun, the observer and the asteroid). More recently, it has been discovered that Barbarian asteroids are also peculiar for exhibiting very large abundances of the spinel mineral in their reflectance spectra [4]. This suggests that Barbarians might be among the most ancient and primitive solid bodies present in our solar system, having been accreted during the very early epochs of formation of the first planetesimals. Their rarity could be interpreted as being due to the fact that only a few objects belonging to this first generation of planetesimals have been lucky enough to survive the early processes that led to the removal of the vast majority of the planetesimals initially accreted between Mars and Jupiter.

An important recent discovery has been that one dynamical family of asteroids, named after the high-inclination asteroid (729) Watsonia, is composed of Barbarian asteroids [5]. This opens new possibilities for a better physical characterization and interpretation of Barbarians by means of polarimetric and visual and near-IR spectroscopy, with potential implications for our general understanding of the early phases of the solar system history.

4. Spectro-polarimetry

Recently, the first pioneering attempts to apply the technique of spectro-polarimetry to asteroid studies have started to give interesting results [6]. In addition to spectral reflectance and phase-dependent polarimetric data, spectro-polarimetry also provides another piece of information, namely the relation between the degree of linear polarization and wavelength. According to the first results, it seems that this new parameter can be used to distinguish between objects having different albedo. Moreover, the fairly complicated variation of the polarization gradient observed at different phase angles seems able to produce some important new constraint to modern models of light-scattering phenomena from planetary surfaces. If the first impressions will be confirmed, spectro-polarimetry might soon become the best and fastest technique for the physical characterization of asteroid surfaces, the most important limitation being that of the need of large telescopes to obtain useful data for faint objects.

5. Summary and Conclusions

Asteroid polarimetry is experiencing in these years a general Renaissance. The important results obtained in this field indicate that it is no longer possible to disregard the study of the polarimetric properties of small solar system bodies, since this is one of the major tools to be exploited for the purposes of physical characterization of these bodies, with immediate applications, as an example, to the topic of defense systems against the impact hazard posed by near-Earth objects. Moreover, polarimetry is also important for taxonomic classification purposes. A first interesting application will be a test of the future taxonomic classification that will be

obtained by the Gaia mission. In particular, it will be interesting to see whether the sampling of the blue part of the reflectance spectrum perfomed by Gaia will be able to produce a distinction between asteroids belonging to the current B taxonomic class, and asteroids that were previously classified as F-class. These objects, which are now included in the modern B-class, are known to exhibit well-defined polarimetric properties that clearly distinguish them with respect to other low-albedo taxonomic classes ([7]).

References

[1] Cellino, A., Bagnulo, S., Gil-Hutton, R., Tanga, P., and Cañada-Assandri, M.: On the calibration of the relation between geoemtric albedo and polarimetric properties for the asteroids, submitted to MNRAS, 2015.

[2] Cellino, A., Ammannnito, E., Magni, G.F., Gil-Hutton, R., Belskaya, I.N., and Tedesco, E. F.: The DAWN exploration of (4) Vesta as the ground truth to interpret asteroid polarimetry, submitted to MNRAS, 2015.

[3] Cellino, A., Belskaya, I.N., Bendjoya, Ph., Di Martino, M., Gil-Hutton, R., Muinonen, K., and Tedesco, E. F.: The strange polarimetric behavior of Asteroid (234) Barbara, Icarus, Vol. 180, pp. 565-567, 2006.

[4] Sunshine, J. M., Connolly, H. C., McCoy, T. J., Bus, S. J., and La Croix, L. M.: Ancient Asteroids Enriched in Refractory Inclusions, Science, Vol. 320, p. 514, 2008.

[5] Cellino, A., Bagnulo, S., Tanga, P., Novaković, B., and Delbò, M.: A successful search for hidden Barbarians in the Watsonia asteroid family, MNRAS Letter, Vol. 439, pp. L75-L79, 2014.

[6] Bagnulo, S., Cellino, A., and Sterzik, M.F.: Linear spectropolarimetry: a new diagnostic tool for the classification and characterization of asteroids, MNRAS Letter, vol. 46, pp. L11-L15, 2014.

[7] Belskaya, I. N., Shkuratov, Yu. G., Efimov, Yu. S., Shakhovskoy, N. M., Gil-Hutton, R., Cellino, A., Zubko, E. S., Ovcharenko, A. A., Bondarenko, S. Yu., Shevchenko, V. G., Fornasier, S., and Barbieri, C.: The F-type asteroids with small inversion angles of polarization, Icarus, Vol. 178, pp. 213-221, 2005.

EPSC Abstracts
Vol. 10, EPSC2015-74, 2015
European Planetary Science Congress 2015

Spectroscopy and photometry of L-type asteroids

P. Tanga (1), M. Devogele (1,2), H. Campins (4), N. Pinilla-Alonso (5), L. Abe (1), Ph. Bendjoya (1), A. Cellino (3), J.P. Rivet (1)
(1) Laboratoire Lagrange UMR7293/CNRS, UNS, Observatoire de la Côte d'Azur (2) Institut d'Astrophysique et de Gèophysique, Liège, Belgium (3) INAF/Osservatorio Astrofisico di Torino, Torino, Italia (4) University of Central Florida Orlando, Florida (5) Department of Earth and Planetary Sciences - University of Tennessee, USA

Abstract

Among L-type asteroids, a peculiar category of objects exists: it includes the so-called "Barbarians", known to have very specific features in the phase-polarization curve. Such objects are thought to contain a high percentage of Calcium-Aluminum-rich-Inclusions, responsible of a spinel absorption feature in the near infrared (around 2.1-2.2 μm). However, Barbarians are also peculiar in some other physical properties: in particular they seem to have unusually high rotation periods, and large amplitude light curves. We started a campaign of NIR spectroscopy and photometry to shed a light on such properties and to compare the Barbarians to the other objects belonging to the same taxonomic type.

1. Properties of the Barbarians

The Barbarians were discovered by A. Cellino with the detection of the first objet giving the name to this category: 234 Barbara. They have a strong polarization parallel to the scattering plane at small phase angles, and a transition to perpendicular polarization at unusually high phase angles. Futher details about their nature are provided in the abstract by [1].

Sunshine et al. (2007) [2] suggested that Barbarians could contain a very high percentage of CAIs (up to 30%), not found in the current meteorite sample. If this was true, they could be very ancient objects, formed in a refractory-rich environment.

Also, it appears that Barbarians have irregular shapes and long rotation periods [3], but such properties are verified on a small sample of objects for which they are available.

We thus decided to run a systematic campaign for the acquisition of NIR spectra at IRTF and of light curves of Barbarians – or candidate Barbarians.

2. Our campaign, preliminary results

We were awarded two nights at IRTF that were fully exploited. During our presentation, we will illustrate the results obtained on the NIR spectra of several L-type asteroids, some of them known to be Barbarians. We will discuss the presence of the spinel absorption and its possible relation to photometric properties and albedo. With our observations we have strongly expanded our knowledge on this category of objects.

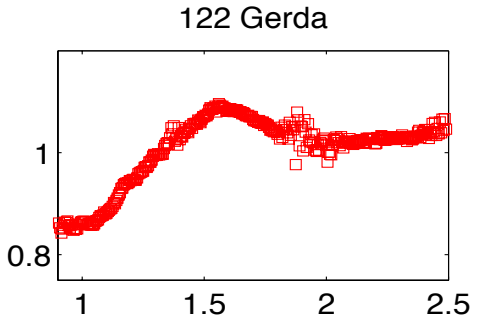

Fig. 1 – Example of spectrum of 122 Gerda, obtained at IRTF by our team. The spinel absorption shows up above 2 μm, over a globally red-sloped spectrum.

References

[1] Cellino, A. et al. 2015, Recent advances in asteroid polarimetry, EPSC 2015

[2] Sunshine, J. et al., 2008, Ancient Asteroids Enriched in Refractory Inclusions, Science, 320, 514

[3] Tanga et al. 2015, The non-convex shape of (234) Barbara, the first Barbarian, MNRAS 448-4, 3382

EPSC Abstracts
Vol. 10, EPSC2015-85, 2015
European Planetary Science Congress 2015

Selection effects in spins and shapes of asteroids

A. Marciniak (1), F. Pilcher (2), D. Oszkiewicz (1), T. Santana-Ros (1), S. Urakawa (3), S. Fauvaud (4,5), P. Kankiewicz (6), K. Kamiński (1), V. Kudak (7) and W. Ogłoza (8);
(1) Astronomical Observatory Institute, A. Mickiewicz University, Poznań, Poland (am@amu.edu.pl), (2) Organ Mesa Observatory, Las Cruces, NM, USA, (3) Bisei Spaceguard Center, Japan Spaceguard Association, Bisei, Japan, (4) Observatoíre du Bois de Bardon, Taponnat, France, (5) Association T60, Toulouse, France, (6) Jan Kochanowski University, Kielce, Poland, (7) Uzhhorod National University, Uzhgorod, Ukraine, (8) Mt. Suhora Observatory, Pedagogical University, Cracow, Poland

Abstract

A problem of observing selection effect in photometric studies of asteroids is sketched. An observing campaign aimed to reduce these effects is described, with its first results concerning corrected period determinations.

Introduction

Physical studies of asteroids strongly depend on lightcurve data. However the abundance of lightcurves for a particular object strongly depends on its physical features like brightness, period of rotation, and lightcurve amplitude.

When the period of rotation is much longer than typical observing run, or the amplitude is close to the noise level, there are difficulties in determining the unique synodic period. However, thanks to the work of dedicated observers, practically all larger main belt asteroids (with absolute magnitude H$\leq$11 mag) have their synodic periods determined with a certain level of confidence (LCDB, [1]). But once the period of rotation is established, and is known to be long, such targets are avoided by most of further observing studies due to instrumental or time limitations. This way their synodic periods often remain unconfirmed by an independent source.

Observing selection effects

Due to such selection effects asteroids with slow rotation (P$\geq$12 hours) and/or rounded shape (a_{max} $\leq$0.25 mag) rarely have enough data to be spin and shape modelled, because there is a lack of data from multiple apparitions and viewing geometries, or the data are of insufficient quality. In spin and shape studies of asteroids, targets with short periods of rotation and large lightcurve amplitudes are thus preferred. This led to the situation displayed in the figure, where a large fraction of population of targets easy to observe and analyse is spin and shape modelled, while the remaining populations are spin and shape modelled in much smaller fraction. As a consequence knowlegde on e.g. spatial spin axis distributions or on asteroid shapes elongation and internal structure can be biased by these selection effects.

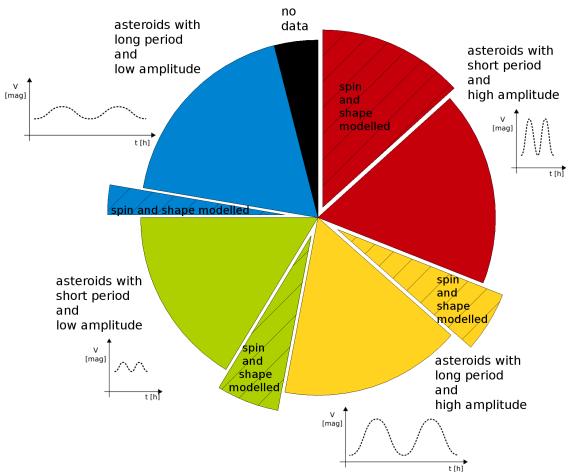

Figure 1: Distribution of periods and amplitudes among all bright (H$\leq$11mag) main-belt asteroids, based on these two parameters simultaneously. A number of spin and shape modelled targets is marked within each group [2].

Initial results

We are conducting an observing campaign of a few dozens of long-period (P$\geq$12 hours) and low amplitude (a_{max} $\leq$0.25 mag) asteroids, aiming to decrease these selection effects. First results of our campaign show that a substantial fraction of periods longer than 12 hours and considered reliable, have actually different values [2]. Around one quarter of studied population displays longer synodic periods than previously accepted, which can somewhat alter e.g. the widely known frequency-diameter plot. Since this fact was found among bright targets, even more profound biases are expected in the range of fainter (smaller) asteroids where observing selection effects are stronger.

We will also present first spin and shape models of our long-period and low-amplitude targets. As judged from their lightcurves, the shapes of these asteroids must be irregular with global asymmetries.

Acknowledgements

This work was partialy supported by grant no. 2014/13/D/ST9/01818 from the National Science Centre, Poland.

References

[1] Warner, B.D., Harris, A.W., Pravec, P.: The asteroid lightcurve database, Icarus 202, p. 134, 2009.

[2] Marciniak, A., Pilcher, F., Oszkiewicz D. et al.: Against the biases in spins and shapes of asteroids, Planet. Space Sci., accepted.

EPSC Abstracts
Vol. 10, EPSC2015-96, 2015
European Planetary Science Congress 2015

The Themis-Beagle families: clues into space weathering processes on primitive asteroids

S. Fornasier (1,2), D. Perna (1), C.Lantz (1,2), M.A. Barucci (1)
(1) LESIA-Observatoire de Paris, France (sonia.fornasier@obspm.fr), (2) Univ Paris Diderot, Sorbonne Paris Cité, France

Abstract

The Themis family is a natural laboratory to study the asteroids-comets continuum and space weathering effects. Recently water ice and organics were detected on 24 Themis indicating that the Themis family may be an important reservoir of ice. Moreover, some main belt comets may be related with the Themis family because of orbital proximities and spectral properties analogies. Within the old Themis family members, a young sub-family, Beagle, formed less than 10 Myr ago, has been identified. Thus the Themis family is very important to shed light on the asteroid-comet continuum, to constrain the abundances of water ices in the outer part of the main belt, and to probe space weathering effects on old Themis and young Beagle families' members.

1. Introduction

Themis is one of the most statistically reliable family in the asteroid belt. First discovered by Hirayama (1918), it has been identified as a family in all subsequent works, and has 550 members as determined by Zappalà et al. [1]. The Themis family is characterized by asteroids with $3.05 \leq a \leq 3.22$ AU, $0.12 \leq e \leq 0.19$, and $0.7^o \leq i \leq 2.22^o$ [2] and spectrally dominated by primitive C- and B-type asteroids, as reported by spectroscopic investigation in the visible range of some members [3,4]. The family formed probably $\sim$ 2.3 Gyr ago as a result of a large-scale catastrophic disruption event of a parent asteroid $\sim$ 400 km in diameter colliding with a 190 km projectile [5]. Interestingly, recent observations by Rivkin and Emery [6] and Campins et al. [7] found spectroscopic evidence of the presence of water ice and organics on the surface of asteroid Themis. Analyzing the infrared spectrum of the asteroid, Rivkin and Emery [6] concluded that the surface of Themis contains very fine water frost, probably in the form of surface grain coatings, and that the infrared spectral signatures can be fully explained by a mixture of spectrally neutral material, water ice, and organics. Contemporaneously, Campins et al. [7] derived that water ice is evenly distributed over the entire Themis surface using spectra obtained at four different rotational phases. Nevertheless the nature of the 3.1 μm feature on 24 Themis is still a matter of debate, and very recently Beck et al. [8] proposed the hydrated iron oxide goethite as alternative interpretation of this feature. However, Jewitt & Guilbert-Lepoutre [9] stress that goethite, when found in meteorites, is a product of aqueous alteration in the terrestrial environment and that extraterrestrial goethite in freshly fallen meteorites is unknown.

The discovery of the presence of water ice and/or hydrated minerals such goethite on 24 Themis indicates that Themis family may be an important reservoir of ice and that possibly ice may exists in the members of the family. Indeed, absorption band in the visible region related to hydrated silicates have been detected on the surface of 15 Themis family members [4]. These materials are produced by the aqueous alteration process, that is a low temperature (< 320 K) chemical alteration of materials by liquid water [10]. The presence of hydrated minerals implies that liquid water was once present on these asteroids, and suggest that post-formation heating took place. Furthermore the Themis family seems to be the source of the main belt comets (MBC) 133P, 238P, 176P, and P/2006 VW139. Nesvorny et al. [11] propose that 133P could potentially be one member of the younger (< 10 Myr) Beagle sub-family of the Themis group. This subfamily has 65 members up to 2 km of diameter.

2. Results

We carried out a spectroscopic survey in the visible and near infrared range at the 3.6 m Italian telescope TNG (la Palma, Spain) during 6 nights in February and December 2012. We got new spectra of 8 Beagle and 22 Themis members using the DOLORES (with the LR-R and LR-B grisms) and the NICS (with the Amici prism) instruments. To look for possible coma around the targets, we also performed deep imaging in

R filter.

All the objects investigated belong to the C or B types. None of the investigated spectra show water ice absorption features at 1.5 and 2 micron, but five Themis members have visible absorption bands associated with hydrated silicates and thus they have experienced the aqueous alteration process in the past.
Spectra of the Themis family members show a range of spectral slope much wider than the Beagle members: 'old' Themis members exhibit a wide range of spectra, including asteroids with blue/neutral and moderately red spectra (relative to the Sun), while the young Beagle members investigated are bluer than the Themis one. The analysis of the spectral slope versus the albedo of the objects, derived from the WISE data, indicates that the young Beagle members are also brighter than most of the old Themis members.
To explain these differences, we propose two possible scenarios: a) The Themis/Beagle family parent body was heterogeneous in composition, and the diversity we see nowdays reflects different source regions in the parent body; b) the family parent body was homogeneous and the spectral variability we see is related to space weathering effects. In the second scenario, our observations imply that on the Themis/Beagle primitive asteroids the space weathering processes acts in a similar way than in silicate rich asteroids, producing a reddening of the spectra and a darkening of the albedo. The analysis of our observations will be presented, and compared to the results of recent laboratory experiments on irradiation of carbonaceous chondrite meteorites.

Acknowledgements

This project was supported by the French Planetology National Programme (INSU-PNP)

References

[1] Zappalà,V., A. Cellino, P. Farinella and Z. Knezevic, 1990, AJ 100, 2030

[2] Zappalà V., Bendjoya P., Cellino A., Farinella P., Froeschle Cl., 1995, Icarus 116, 291

[3] Mothè–Diniz, T., Roig F, Carvano, J.M., 2005, Icarus 174, 54

[4] Florczak M., Lazzaro, D., Mothè–Diniz, Angeli, CA, Betzler A.S., 1998, A&A Supp. Ser. 134, 466

[5] Marzari, F., Davis D., Vanzani, V. 1995, Icarus 113, 168

[6] Rivkin, A.S., Emery, J.P. 2010, Nature 464, 1322

[7] Campins, K. Hargrove, N. Pinilla-Alonso, E.S. Howell, M.S. Kelley, J. Licandro, T. Mothè-Diniz, Y. Fernandez and J. Ziffer, 2010, Nature 464, 320

[8] Beck,P., Quirico, E., Sevestre, D., Montes-Hernandez,D., Pommerol A., Schmitt, B., 2011, A&A 526, A85

[9] Jewitt & Guilbert-Lepoutre, 2012, AJ, 143, 21

[10] Vilas F., Sykes M.V., 1996, Icarus 124, 483

[11] Nesvorny, D., W.F. Bottke, D. Vokrouhlicky, M. Sykes, D.J. Lien and J. Stansberry, 2008, AJ 679, 143

EPSC Abstracts
Vol. 10, EPSC2015-137, 2015
European Planetary Science Congress 2015

Thermal Cracking of the asteroid (3200) Phaethon and the Origin of the Geminid Meteors

M. Delbo (1), J. Wilkerson (2) G. Libourel (1) V. Ali-Lagoa (1) , J. Hanus (1), and P. Michel (1)
(1) Observatoire de la Cote d'Azur - Boulevard de l'Observatoire - CS 34229 - F 06304 NICE Cedex 4 (marcodelbo@gmail.com).
(2) Department of Mechanical Engineering The University of Texas at San Antonio One UTSA Circle San Antonio, TX 78249

Abstract

We investigate the importance of thermal cracking of the near-Earth asteroid (3200) Phaethon for the origin of the Geminid meteors. This is the densest annual meteoroid stream and potential meteorite dropper. Geminds are associated with Phaethon. The latter is likely a chip of the large main-belt asteroid (2) Pallas. Different models have been investigated for the origin of the Geminids, but none of these resulted completely satisfactory to explain the formation of this massive meteor stream.

1. Introduction

While meteor streams are in general associated with comets, the Geminids, which have their yearly peak activity near December 13, are parented by the unusual near-Earth asteroid (NEA) 3200 Phaethon [1].

Phaethon's nature has always been mysterious: while comet nuclei release material due to the sublimation of volatile species, leaving behind dust particles that become meteors when they encounter Earth's atmosphere, most of NEAs do not have activity [2]. Because Phaeton did show activity, it was initially thought to be dormant comet. However, spectroscopic observations showed that Phaethon has an extremely blue reflectance spectrum [3], whereas comet nuclei are usually very red [4]. This observation argued against a cometary nature of Phaethon. Further spectroscopic and dynamical investigation suggested a link with the asteroid (2) Pallas and its collisional family [5]. Moreover, the Geminids have composition and densities consistent with some carbonaceous chondrites that are believed to be of asteroidal origin [6]. From bolide observations, the same authors also pointed out that the Geminids may drop meteorites [6], leading to the tantalising idea that we can receive pieces of Pallas on Earth.

After several attempts, recent observations confirmed the activity of Phaethon near perihelion [7]. The activity was only 10^{-4} of the Geminid stream mass, but, quoting [8], "this raises the possibility that the decay of Phaethon is a continuing process" .This is the position along its orbit where dynamical calculations have shown that the Geminids had to be released [9]. However, the mechanisms responsible for the productions and release of dust from Phaethon remain unknown, albeit several hypothesis have been put forward [8].

1.1. Phaethon's orbit and temperatures

Phaethon has an extremely eccentric orbit, that brings the body at 0.14 au at perihelion, where its surface temperature can reach more than 1000 K (see Fig. 1).

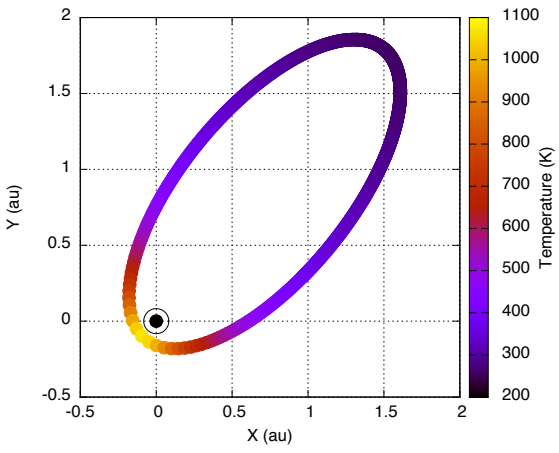

Figure 1: The orbit of Phaethon projected on the plane of the ecliptic. A circle is drawn every day. The colour of the circle gives the asteroid surface temperature at the sub-solar point.

2. Thermal Cracking

It has been recently shown that the variation of the temperatures due to diurnal illumination cycle on asteroids induce thermal fatigue of the surface material [10]. Thermal fatigue is the progressive growth of cracks caused by temperature gradients and differential temperature expansions in inhomogeneous materials, both resulting in mechanical stresses. Eventually cracks reaches a critical size and the material fragment. This is a very effective regolith production mechanisms. It was estimated that for NEAs, mars-crosser and for the inner Main Belt asteroids, thermal cracking produces regolith faster than micrometeorite bombardment, the classical process invoked for regolith formation and development on asteroids [11].

The velocity of crack propagation and thus the time needed for a crack to grow from the surface through the entire rock so that it becomes fragmented, is a strong function of the distance of the asteroid from the sun [10].

2.1. Thermal Cracking at Phaethon's perihelion

We will show here that the rock survival time, or the time it takes a crack to grow through the rock is proportional to $(\Delta T)^{-n}$ where ΔT is the day-to-night excursion temperature on the asteroid and n is the exponent of the Paris law that governs the crack growth rate. In particular, since the rock survival time at 1 au is of the order of 10^4 year for carbonaceous mineralogies and the exponent $n \sim 4$ [10], the rock survival time on Phaethon is of the order of few years at the perihelion temperatures.

Moreover, regolith production by thermal cracking is a continuos process, whose rate strongly increases near each perihelion passage.

We will investigate if and how rock break up at each perihelion passage can produce fresh regolith, a potential source of material to explain the Geminids.

Acknowledgements

This work is supported by the French Agence National de la Recherche (ANR) SHOCKS.

References

[1] I. P. Williams and Z. Wu, "The Geminid meteor stream and asteroid 3200 Phaethon," *Monthly Notices of the Royal Astronomical Society (ISSN 0035-8711)*, vol. 262, pp. 231–248, May 1993.

[2] D. Jewitt, H. Hsieh, and J. Agarwal, "The Active Asteroids," in *Asteroids IV*, University of Arizona Press, Tucson, AZ, Sept. 2015.

[3] J. Licandro, H. Campins, T. Mothé-Diniz, N. Pinilla-Alonso, and J. de León, "The nature of comet-asteroid transition object (3200) Phaethon," *Astronomy and Astrophysics*, vol. 461, pp. 751–757, Jan. 2007.

[4] H. Campins, J. Ziffer, J. Licandro, N. Pinilla-Alonso, Y. Fernández, J. d. León, T. Mothé-Diniz, and R. P. Binzel, "Nuclear Spectra of Comet 162P/Siding Spring (2004 TU12)," *The Astronomical Journal*, vol. 132, pp. 1346–1353, Sept. 2006.

[5] J. de León, H. Campins, K. Tsiganis, A. Morbidelli, and J. Licandro, "Origin of the near-Earth asteroid Phaethon and the Geminids meteor shower," *Astronomy and Astrophysics*, vol. 513, p. A26, Apr. 2010.

[6] J. M. Madiedo, J. M. Trigo-Rodriguez, A. J. Castro-Tirado, J. L. Ortiz, and J. Cabrera-Caño, "The Geminid meteoroid stream as a potential meteorite dropper: a case study," *Monthly Notices of the Royal Astronomical Society*, vol. 436, pp. 2818–2823, Dec. 2013.

[7] D. Jewitt and J. Li, "Activity in Geminid Parent (3200) Phaethon," *The Astronomical Journal*, vol. 140, pp. 1519–1527, Nov. 2010.

[8] D. Jewitt, "The Active Asteroids," *The Astronomical Journal*, vol. 143, p. 66, Mar. 2012.

[9] B. A. S. Gustafson, "Geminid meteoroids traced to cometary activity on Phaethon," *Astronomy and Astrophysics*, vol. 225, pp. 533–540, Nov. 1989.

[10] M. Delbo, G. Libourel, J. Wilkerson, N. Murdoch, P. Michel, K. T. Ramesh, C. Ganino, C. Verati, and S. Marchi, "Thermal fatigue as the origin of regolith on small asteroids," *Nature*, vol. 508, pp. 233–236, Apr. 2014.

[11] F. Hörz and M. Cintala, "Impact experiments related to the evolution of planetary regoliths," *Meteoritics & Planetary Science*, vol. 32, pp. 179–209, Mar. 1997.

EPSC Abstracts
Vol. 10, EPSC2015-138, 2015
European Planetary Science Congress 2015

Ion irradiation of carbonaceous chondrites as a simulation of space weathering on C-complex asteroids

C. Lantz (1,2), R. Brunetto (3), M.A. Barucci (1), C. Bachelet (4), D. Baklouti (3), J. Bourçois (4), E. Dartois (3), J. Duprat (4), P. Duret (3), C. Engrand (4), M. Godard (4), D. Ledu (4), O. Mivumbi (3), and S. Fornasier (1)

(1) LESIA – Observatoire de Paris, CNRS / UPMC Univ. Paris 6 / Univ. Paris Diderot, Meudon, France, (2) Université Paris Diderot, Sorbonne Paris Cité, Paris, France (cateline.lantz@obspm.fr), (3) IAS, CNRS / Université Paris Sud, Orsay, France, (4) CSNSM, IN2P3 – CNRS / Université Paris-Sud, Orsay, France

Abstract

We are investigating the effects of space weathering on primitive asteroids using ion irradiation on their meteoritic analogs. To do so, we exposed several carbonaceous chondrites (CV Allende, COs Lancé and Frontier Mountain 95002, CM Mighei, CI Alais, and ungrouped Tagish Lake) to 40 keV He^+ ions as a simulation of solar wind irradiation using fluences up to 6.10^{16} ions/cm^2 (implantation platform IRMA at CSNSM Orsay). As a test for our new experimental setup, we also studied samples of olivine and diopside. We confirm the reddening and darkening trends on S-type objects, but carbonaceous chondrites present a continuum of behaviors after ion irradiation as a function of the initial albedo and carbon content: from red to blue and from dark to bright.

1. Introduction

The exposition of airless bodies to the harsh environment in which they evolve (solar ion irradiations, micrometeorite bombardments, etc.) leads to surface alterations affecting spectra. This phenomenon is known as space weathering (SpWe). Lot of studies have been made on S-type asteroids and silicate materials, including laboratory experiments [1] and direct confirmation on Itokawa grains [2] of the well know darkening and reddening trends. On the contrary, few results have been obtained on C-type asteroids and no general trend has been found [3-5]. In order to understand the influence of SpWe on primitive asteroids, we conduct laboratory simulations on carbonaceous chondrites. The goal is to develop a model of SpWe which will also support sample return missions (OSIRIS-REx/NASA and Hayabusa-2/JAXA).

2. Previous experiment

In a first step, we exposed fragments of CV Allende [6] and CM Murchison [7] to 40 keV He^+ and Ar^+ (fluences up to 3.10^{16} ions/cm^2, platform SIDONIE at CSNSM). They showed different spectral behaviors after irradiation in the 0.425-1.25µm range. Allende clearly reddened and darkened while Murchison had small spectral variations difficult to interpret taking into account the sample heterogeneity concern. It appeared clearly on both samples that in the 10 µm region, bands of silicates and/or phyllosilicates move toward longer wavelength {Fig.1}. Murchison, which is an aqueous altered meteorite, also presents a band shift in the 3 µm region. These modifications toward the Fe-rich spectral region suggesting a loss of the element Mg are probably due to a preferential sputtering of Mg and/or amorphization of Mg-rich materials. These results cannot confirm the presence of npFe0, but do not disagree with the forming mechanism [8].

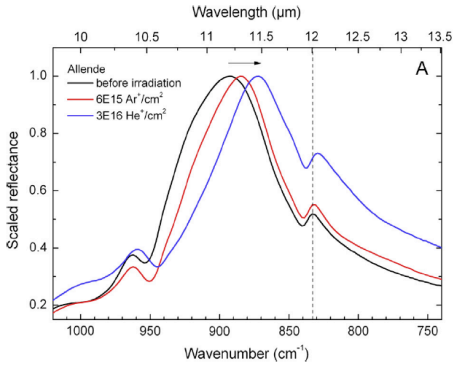

Figure 1: MIR confocal reflectance spectra (SMIS beam line at Synchron SOLEIL) of Allende around the silicate peak at 11 µm before and after the highest irradiation doses for both ions. Figure from Brunetto et al. 2014.

3. Comparison with other ion irradiations

We put together the results of other ion irradiations made by different teams [1, 3, 6, 7, 9]. We observe two distinct behaviours {Fig.2}. On one hand there are the brighter materials like ordinary chondrites (and olivine) showing clearly the well known darkening and reddening effects. On the other hand, we find the carbonaceous chondrites with transitional

trend that seems to depend on the original composition.

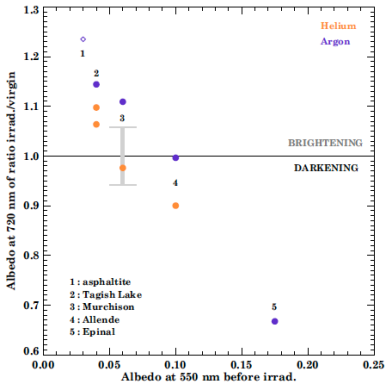

Figure 2: Reflectance of ratioed spectra (irradiated/unirradiated) as a function of the initial albedo. The grey error bar indicates the variations due to our Murchison sample heterogeneity. Figure from Lantz et al. 2015.

4. This new study

We use a new vacuum chamber (project INGMAR) to perform spectroscopic studies from 0.4 to 2.5 µm. This setup allows us to collect diffuse reflectance spectra of the same region of the sample as a function of the increasing dose (fluences of 5.10^5, 1.10^6, 3.10^6, and 6.10^6 He^+/cm^2 are used here). An example is given in Fig.3 for irradiated olivine, where reddening and darkening are seen.

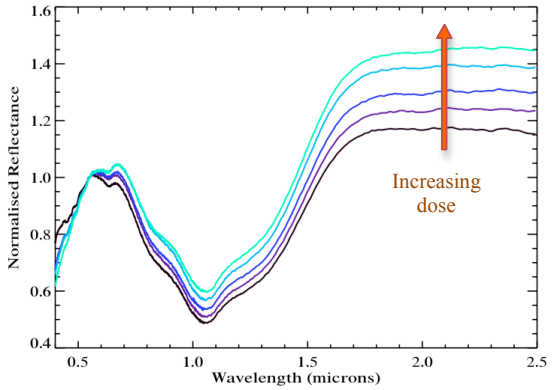

Figure 3: Spectra before and after irradiations (the brighter color, the stronger dose) for olivine.

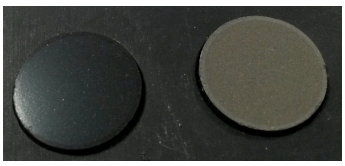

Figure 4: Pellets (13mm in diameter) of CM Mighei (left) and CO Lancé (right). On the edge of the pellet, one can see an unirradiated area (corona of 500 µm): the altered region gets darker for the CO and brighter for the CM.

Irradiated pellets of olivine, diopside, CV and CO meteorites show spectral reddening and darkening in the VIS-NIR, while the darker meteorites tend to brighten, as seen in Fig.4, and get bluer spectra after irradiation.

Preliminary results in the MIR range show for all the carbonaceous chondrites and the silicate samples a shift toward longer wavelength of the silicate/phyllosilicate bands as seen in our previous study on Allende and Murchison. The aqueous altered meteorites also suffer a modification of the dedicated 3 µm band.

Acknowledgements

We warmly thank the Natural History Museum of Vienna, the Vatican Observatory, J. Brucatto, D. Cruikshank and L. Folco for providing us with the meteorite samples. We are grateful to D. Fulvio for sharing data, to A. Arondel, P. Blache, S. Blivet, and F. Fortuna for their contribution to the conception of the experimental setup, to F. Borondics and C. Sandt for their help and support at the SMIS beamline of the Synchrotron SOLEIL, and to P. Beck, L. Bonal, and E. Quirico for useful discussions.
This research is part of a joint IAS-CSNSM project (INGMAR) and it has been funded by the French national program "Programme National de Planétologie" (PNP), by the Faculté des Sciences d'Orsay, Université Paris-Sud ("Attractivité 2012"), by the French National Research Agency "Agence Nationale de la Recherche" (contract ANR-11-BS56-0026, OGRESSE), and by the P2IO LabEx (ANR-10-LABX-0038) in the framework "Investissements d'Avenir" (ANR-11-IDEX-0003-01) managed by the French National Research Agency (ANR).

References

[1] Brunetto, R., Vernazza, P., Marchi, S., et al.: Modeling asteroid surfaces from observations and irradiation experiments: The case of 832 Karin, Icarus, Vol. 184, pp. 327-337, 2006.
[2] Hiroi, T., Abe, M., Kitazato, K., et al.: Developing space weathering on the asteroid 25143 Itokawa, Nature, Vol. 443, pp. 56-58, 2006.
[3] Moroz, L., Baratta, G., Strazzulla, G., et al.: Optical alteration of complex organics induced by ion irradiation: 1. Laboratory experiments suggest unusual space weathering trend, Icarus, Vol. 170, pp. 214-228, 2004.
[4] Lazzarin, M., Abe, M., Kitazato, K., et al.: Space weathering in the Main Atseroid Belt: The big picture, ApJ, Vol. 647, pp. 179-182, 2006.
[5] Lantz, C., Clark, B.E., Barucci, M.A., and Lauretta, D.S: Evidence for the effects of space weathering spectral signatures on low albedo asteroids, A&A, Vol. 554, A138, 2013.
[6] Brunetto, R., Lantz, C., Ledu, D., et al.: Ion irradiation of Allende meteorite probed by visible, IR, and Raman spectroscopies, Icarus, Vol. 237, pp. 278-292, 2014.
[7] Lantz, C., Brunetto, R, Barucci, M.A., et al.: Ion irradiation of the Murchison meteorite: Visible to mid-infrared spectroscopic results, A&A, *in press*, 2015.
[8] Hapke, B.: Space weathering from Mercury to the asteroid belt, JGR, Vol. 106, pp. 10039-10073, 2001.
[9] Vernazza, P., Fulvio, D., Brunetto, R., et al.: Paucity of Tagish Lake-like parent bodies in the Asteroid Belt and among Jupiter Trojans, Icarus, Vol. 225, pp. 517-525, 2013.

EPSC Abstracts
Vol. 10, EPSC2015-173, 2015
European Planetary Science Congress 2015

A perspective of the Ceres' missing family

A. Migliorini (1), M.C. DeSanctis (1), R. Duffard (2), N. Pinilla-Alonso (3) and D. Lazzaro (4)
(1) Institute of Space Astrophysics and Planetology, INAF, Rome, Italy, (2) IAA Granada, Spain, (3) Earth and Planetary Sciences Department, University of Tennessee, USA, (4) National Observatory of Rio, Rio de Janeiro, Brazil

(alessandra.migliorini@iaps.inaf.it, fax: +39-06-45488188)

Abstract

Ceres was recently linked to the dynamical family 93 (Milani et al. 2014). However, asteroids belonging to this family are likely to be S-type, while Ceres is a C-type. Different scenarios, dealing with a catastrophic disruption, compositional heterogeneity on the Ceres surface, or the overlapping of families with different origin, could explain this diversity.
We propose to spectroscopically characterize family 93 to add physical information that help constraining the dynamical models, through data acquired from ground-based and from space telescopes in the infrared.

1. Introduction

The classification of numbered asteroids in dynamical families, proposed by Milani et al. (2014), identifies 19 dynamical families with more than 1000 members, and several medium to small families. However, one major issue of this study is the missing family of Ceres, despite the large size of the body. According to dynamical hypothesis, family 93 could be the source of bodies where we should look for the ancient Ceres' family. The family 93 counts about 1800 members, part of which could be the result of an impact event on Ceres' surface (Milani et al. 2014).

Ceres and 93 Minerva are spectroscopically classified as C-type asteroids with an albedo lower than 0.1 (Li et al. 2006). However, family 93 includes asteroids quite different one another and also different from 93 Minerva, their parent body, and Ceres. Most of them show an albedo higher than 0.1 (Wright et al. 2010). For this reason, the identification of the family is quite difficult, and it was revised several times during the last decades. This asteroid group was formerly classified as the Ceres family (Zappalà et al. 1995) and as the Gefion family (Bus 1999). Subsequently, asteroid 93 Minerva was identified as the parent body of this family (Mothé-Diniz et al. 2005); in their classification the family counts 865 members, 34 of which have an associated spectroscopic classification. The majority of these asteroids belong to the S-complex (precisely 26 S class, 2 Sl class, 2 Sr class, 1 Sq class, and 1 L class), while 2 asteroids belong to the C complex (1 Cb class and 1 Ch class), and finally there is one X class asteroid. This seems to contradict the hypothesis proposed in Milani et al. (2014) but at the same time arises a big question on the possible link between Ceres, family 93 and its parent body.

2. Data analysis

To search for Ceres' family, we study the spectral properties of low albedo primitive asteroids, in comparison to Ceres and Minerva. Data were selected from the available ground-based dataset. In addition, a comparison with vis-NIR spectra acquired with the VIR instrument (De Sanctis et al. 2011) on board the NASA DAWN mission (Russell and Raymond, 2011) may shed light on the relationship between Ceres and the primitive asteroids belonging to family 93. It is worth noting that the Ceres and Minerva vis-NIR spectra show some differences (see Figure 1). VIR data, acquired while approaching Ceres and during the early phases of the spacecraft orbit about the body, could be used to associate the rest of the primitive asteroids in 93 family with Ceres or Minerva as parent bodies.

Spectral slope in the infrared is quite peculiar in the Ceres and Minerva, as shown in Figure 1. Hence, this parameter, together with the low albedo, can be used as a diagnostic to infer if an asteroid can belong to the Ceres' family. The same parameter will enable us to discriminate among C-type asteroids.

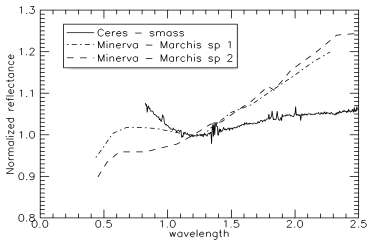

Figure 1: Comparison between the spectra of Ceres and Minerva.

A proposal for new observations of selected asteroids from the family 93 was submitted to IRTF for the next observing period. This will complement the literature investigation with new and dedicated observations.

6. Summary and Conclusions

The present investigation is done using archive data of primitive asteroids associated with the family of 93 Minerva, in comparison to the VIR data acquired in the recent observing campaign of Ceres. In combination with a campaign of ground-based observations that is on-going, it attempts to answer to the intriguing question about the missing family of Ceres. Our immediate objectives can be summarized as follows:

1) Search for the Ceres family, by investigating the spectral propertied of low albedo asteroids in comparison to the Ceres' spectra provided by VIR at DAWN.

2) Characterize, at the same time, asteroids belonging to the Minerva family, through the investigation of differences in the spectral properties.

3) Study the distribution of C and S type asteroids in the region from 2.5 AU to 2.8 AU, where Ceres and the family 93 are located.

Acknowledgements

This work was supported by the Italian Space Agency (ASI), ASI-INAF Contract I/004/12/0. Support of the Dawn Science, Instrument, Operations Teams, as well as of the Dawn at Vesta Participating Scientist program, is gratefully acknowledged.

References

[1] Milani A., Cellino A., Knežević Z., Novaković B., Spoto F. Paolocchi P., Asteroid families classification: Exploiting very large datasets, Icarus 239, 46.73, 2014.

[2] Li Y.-J., McFadden L.A., Parker J.W, Young E.F., Stern S.A., Thomas P.C., Russell C.T., Sykes M.V., Photometric analysis of 1 Ceres and surface mapping from HST observations, Icarus, 182, 143-160, 2006.

[3] Wright E.L. et al., The Wide-field Infrared Survey Explorer (WISE): Mission description and initial on-orbit performance, The Astronomical Journal, 140, 1868-1881, 2010.

[4] Zappala V., Bendjova Ph., Cellino A., Farinella P. Froeschlé C., Asteroid families: Search of a 12,487-asteroid sample using two different clustering techniques, Icarus 116, 291-314, 1995.

[5] Bus S.J., PhD Thesis MIT, 1999.

[6] Mothé-Diniz T., Roig F., Carvano J.M., Reanalysis of asteroid families structure through visible spectroscopy, Icarus 174, 54-80, 2005.

[7] De Sanctis M.C., Coradini A., Ammannito E., Filacchione G., Capria M.T., Fonte S., Magni G. Barbis A., Bini A., Dami M., Ficai-Veltroni I., Preti G., The VIR Spectrometer, Space Science Reviews 163, 329-369, 2011.

[8] Russell C.T. and Raymond C.A., The Dawn Mission to Vesta and Ceres, Space Science Reviews 163, 3-23, 2011.

EPSC Abstracts
Vol. 10, EPSC2015-196, 2015
European Planetary Science Congress 2015

Color and Space Weathering on Lutetia

S.E. Schröder (1), H.U. Keller (1,2), S. Mottola (1), F. Scholten (1), F. Preusker (1), K.-D. Matz (1), and S. Hviid (1)
(1) Deutsches Zentrum für Luft- und Raumfahrt (DLR), 12489 Berlin, Germany (stefanus.schroeder@dlr.de), (2) Institut für Geophysik und extraterrestrische Physik (IGEP), Technische Universität Braunschweig, 38106 Braunschweig, Germany

1. Introduction

During the flyby in 2010, the OSIRIS camera on-board Rosetta acquired hundreds of high-resolution images of asteroid Lutetia's surface through a range of narrow-band filters. While Lutetia appears very bland in the visible wavelength range, UV color variations were tentatively identified in the Baetica crater cluster (Fig. 1) [1]. As Lutetia remains a poorly understood asteroid, such color variations may provide clues to the nature of its surface. We take the analysis one step further and study color and albedo variability at a much higher spatial resolution than before.

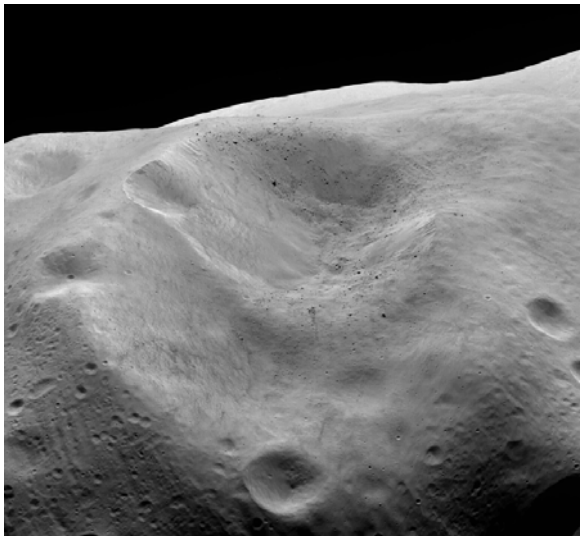

Figure 1: The crater complex in the Baetica region in which color variations were tentatively identified [1].

2. Method

We concentrate our analysis on sets of images in which the images were taken through a sequence of color filters in rapid succession, such that the changes in phase angle and distance to the asteroid are small within the set. We orthorectify the images using the shape model and improved orientation data (orbit position and pointing) that were derived by stereo-photogrammetric analysis [2]. We compensate for the effects of illumination and local topography by photometrically correcting the images. Alternatively, we apply a principal component analysis (PCA) to isolate subtle color variations by eliminating apparent brightness variations due to topography and albedo.

3. Color variations

First we photometrically correct the images with the Hapke model [3]. We find that subtle color variations are associated with the Baetica region (Fig. 2), where the interior of the central crater has an orange tint and a major landslide (*Danuvius Labes*) appears blue.

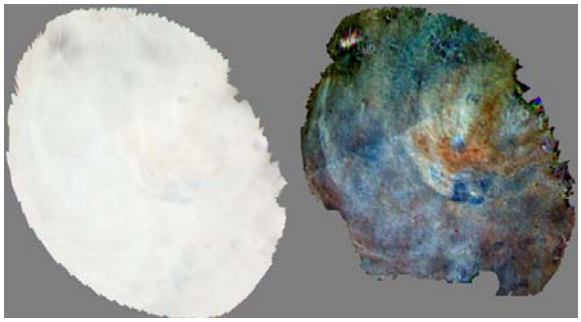

Figure 2: Color composites of the Baetica crater complex. At left a composite of the absolute reflectance, at right a composite of photometrically corrected images (contrast enhanced).

With the PCA we can separate brightness from color variations. The former are isolated in the first principal component whereas the latter are isolated in the higher components (Fig. 3). The associated eigen-vectors show us the spectral nature of the dominant color variations. The PCA confirms that the bottom part of the crater cluster is the site of a major landslide that is bluer and darker than average. The top part of the cluster is redder and brighter than average with streaks of material that are oriented radially to the cluster center. We identify these streaks as crater rays.

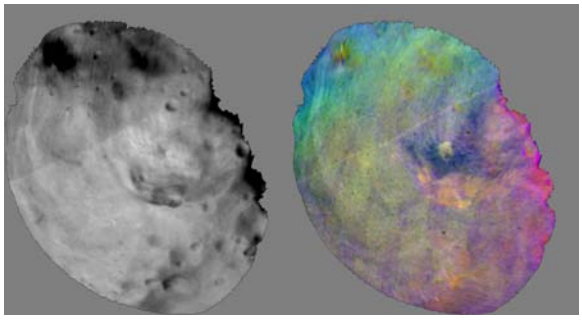

Figure 3: Principal component analysis of a color cube acquired at low phase angle. At left the first principal component, at right a color composite of components 2, 3, and 4.

We interpret the color and albedo variability in terms of the degree of soil maturation, or space weathering, where bright and blue equals fresh and dark and red equals mature. We envision the following scenario: An impact created the central crater and covered the crater floor with a reddish material of either endogenous or exogenous origin. The large landslide postdates the impact and has exposed blue, fresh material.

4. Summary

We analyze subtle color and albedo variations on the surface of asteroid Lutetia as seen by the Rosetta OSIRIS camera. We employ various techniques like photometric correction and principal component analysis. The variations can at least partly be explained in terms of space weathering.

References

[1] Magrin, S., La Forgia, F., Pajola, M., Lazzarin, M., Massironi, M., Ferri, F., da Deppo, V., Barbieri, C., Sierks, H., and the Osiris Team: (21) Lutetia spectrophotometry from Rosetta-OSIRIS images and comparison to ground-based observations. P&SS 66, pp. 43–53, 2012.

[2] Preusker, F., Scholten, F., Knollenberg, J., Kührt, E., Matz, K.-D., Mottola, S., Roatsch, T., and Thomas, N.: The northern hemisphere of asteroid (21) Lutetia - topography and orthoimages from Rosetta OSIRIS NAC image data. P&SS 66, pp. 54–63, 2012.

[3] Hapke, B.: Theory of Reflectance and Emittance Spectroscopy. Cambridge University Press, 1993.

EPSC Abstracts
Vol. 10, EPSC2015-220, 2015
European Planetary Science Congress 2015

The dramatic event of the 2029 close encounter (CE) between the Earth and the asteroid (99942) Apophis on April 13th.,2029 at a minimum distance of roughly 38 400 km constitutes an opportunity to deepen investigations concerning the orbital and rotational changes of an asteroid during such an event.

Here, after summarizing the changes undergone by the asteroid orbital elements during the CE we evaluate the rotational changes of Apophis caused by tidal gravitational effects. In particular we take into account not only the effects due to the dynamical flattening of Apophis but also the effects due to its triaxial form, on the precession-nutation motion of the axis of rotation in space. Moreoever we compute what should be the modifications of the angular rate of rotation due to tidal deformation. Our method is based on the determination of the disturbing potential due to the Earth, depending both on the asteroid flattening and triaxiality. Moreoever we estimate what should be the zonal deformation of the asteroid due to the tide exerted by the Earth.

As results, we show that the variations of obliquity and precession in longitude of Apophis during the 2029 close encounter can reach very large values, at the level of 10° or more, depending on the initial values of a few physical and geometrical parameters. On the contrary, variations of the spin rate should be relatively small, but not negligible in view of the expected radar observations
.

EPSC Abstracts
Vol. 10, EPSC2015-223, 2015
European Planetary Science Congress 2015

Bayesian statistical approach to binary asteroid orbit determination

I.D. Kovalenko (1), R.S. Stoica (2), D. Hestroffer (1), A. Doressoundiram (1)
(1) Paris Observatory, France, (2) Lille 1 University, France (ikovalenko@imcce.fr)

Abstract

Orbit determination from observations is one of the classical problems in celestial mechanics. Here we present a statistical approach to banary asteroids orbit determination based on the algorithm of Monte Carlo Markov Chain (MCMC). Furthermore, the present method can be used on the orbit determination in the Gaia mission program for the observations of binary asteroids.

1. Introduction

The study of binary asteroids is of particular interest because the process of their formation and evolution have began since the formation of the Solar System. Therefore, the detection of large number of them and their study may have important implications for understanding and verifications of theoretical models of dynamical evolution of the Solar System. the determined orbit allows to derive the mass, and consequently the density if the size is known, which are essential physical characteristics of objects.
Calculate the orbit of a single asteroid with great accuracy is much easier than the orbit of binaries and this problem is complicated by relative motion of its components. Orbit determination is an inverse problem: we determine orbital parameters from observations.

2. Orbital parameters and observations

Every complete observation of a visual binary asteroid supplies with three data: the time of observation t, the position angle θ of the secondary asteroid with respect to the primary, and the angular distance ρ between the two asteroids. The given coordinates are measured in the tangent plane which changes for each observation. We introduce a coordinate frame related to the tangent plane, where x-axis is directed to the North, the y-axis to the Est and the third z-axis is normal to the tangent plane and directed towards observer, and we transform visually observed coordinates of secondary asteroid with primary asteroid in the origin to rectangular coordinates x, y:

$$\begin{aligned} x &= \Delta\delta = \rho\cos\theta \\ y &= \Delta\alpha\cos\delta = \rho\sin\theta \end{aligned} \tag{1}$$

The elements which define the relative orbit are the six Keplerian elements $(a, e, i, \Omega, \omega, T)$ and the period of revolution P. The semi-major axis a and eccentricity e define the form and the size of the orbit's ellipse, the inclination i, the longitude of the ascending node Ω and the argument of periapsis ω define the the position of orbit plane relatively to the equatorial frame, the time of periapsis passage and the period define the relative position of components at specific time.

3. Statistical inversion problem

The statistical ranging method for simple asteroids has been investigated by J.Virtanen et al. [2] and was applied for binary asteroids relative orbit determination by D.Oszkievicz et al. [1]. The main distinction of our method consists in the choice of proposal orbits: on each iteration we vary directly the orbital parameters to fit a new orbit, while in the previous methods proposal orbits derived through the sampling of observational coordinates. Moreover, compared to [1] algorithm, we combine MCMC method with the simulated annealing for the global optimization problem in order to find the best solution.

3.1. Bayesian statistical approach

The input data are made of N observations at times $t = (t_1, ..., t_N)$, which are related with theoretical positions by the observational equation:

$$\varphi = \psi(S) + \varepsilon \tag{2}$$

$$\varphi = (x_1, y_1; ...; x_N, y_N) \tag{3}$$

$$S = (a, e, i, \Omega, \omega, T, P) \tag{4}$$

$$\varepsilon = (\varepsilon_{\rho 1}, \varepsilon_{\theta 1}; ...; \varepsilon_{\rho N}, \varepsilon_{\theta N}) \quad (5)$$

where φ is a set of N observations coordinates on the tangent plane. $\psi(S)$ is a computed sky-plane positions, S the orbit determination parameters, ε contains the observational errors.

The problem leads to determination of the conditional probability density of the elements S with given observations φ, that is the *a posteriori* probability. Using the Bayes theorem and assuming that the probability density of observations $p(\varphi)$ is invariant for any orbits , the *a posteriori* probability density of the elements is related to the *a priori* probability and the likelihood probability:

$$p(S|\varphi) \propto p(S)p(\varphi|S) \quad (6)$$

3.2. MCMC method

We use the Metropolis–Hastings algorithm with the simulated annealing in order to obtain a sequence of orbits through sampling parameters S. Thus, for each iteration t randomly generate a candidate set of parameters S' from a proposed distribution $Q(S' \rightarrow S_{t-1})$. Namely, we introduce uniform random deviates with a small variation of each parameter around the last accepted sampling. The acceptance criteria:

$$\alpha = \min \left\{ 1, \left[\frac{p(S'|\varphi)}{p(S_t|\varphi)} \right]^{1/T} \frac{Q(S_t \rightarrow S')}{Q(S' \rightarrow S_t)} \right\} \quad (7)$$

where $T = h(T)$, called the temperature, is a global time-varying parameter. Each new orbit is accepted $S_t = S'$ with probability α. The acceptance ratio α indicates how probable the new proposed orbit is, according to the distribution $p(S|\varphi)$. Thus, we will tend to stay in high-density regions of $p(S|\varphi)$.

4. Summary and Conclusions

The MCMC method in form of the Metropolis–Hastings algorithm, adding a globally convergent coefficient, allows to derive one orbit with the biggest probability density of orbital elements. Additionally, the sequence of possible orbits derives through the sampling of each orbital parameter determines the phase space of every possible orbit considering each parameter. Thus the proposed method can be used for the preliminary orbit determination with relatively small number of observations, or for adjustment of orbit previously determined. The Gaia mission will provide positional measurements with high accuracy, which we will use for orbit determination. Asteroid binaries with large ($\approx$ 100 km) and small ($\leq$ 10 km) primary bodies will be observed in the course of the Gaia program. For those objects improved orbits, and consequently masses can be computed using our proposed method.

Acknowledgements

This work is supported by Labex ESEP (ANR N° 2011-LABX-030).

References

[1] D. Oszkiewicz, K. Muinonen, J. Virtanen, and M. Granvik. Asteroid orbital ranging using Markov-Chain Monte Carlo. Meteoritics and Plan- etary Science, 44:1897–1904, Jan. 2009.

[2] J. Virtanen, K. Muinonen, and E. Bowell. Statistical Ranging of Asteroid Orbits. Icarus, 154:412–431, Dec. 2001.

EPSC Abstracts
Vol. 10, EPSC2015-335, 2015
European Planetary Science Congress 2015

The NEOShield-2 EU Project

E. Dotto (1), E. Perozzi (2,3,4), M. Micheli (3,4,5), S. Ieva (1), A. Di Paola (1), M. Cortese (2,6), B. Borgia (3,5), D. Perna (7), E. Mazzotta Epifani (1), R. Speziali (1), M. Lazzarin (8), I. Bertini (8), S. Magrin (8)

(1) INAF-Osservatorio Astronomico di Roma, I, (2) Deimos Space , RO, (3) ESA-NEOCC, I, (4) INAF-IAPS Roma,I, (5) SpaceDyS, I, (6) Università di Tor Vergata, Roma, I, (7) LESIA- Observatoire de Paris, F, (8) Università di Padova, I (elisabetta.dotto@oa-roma.inaf.it /Fax:+39 06 9447243)

Abstract

The NEOShield-2 (2015-2017) project has been recently approved by the European Commission in the framework of the Horizon 2020 programme with the aims

- to study specific technologies and instruments to conduct close approach missions to NEOs or to undertake mitigation demonstration, and
- ii) to acquire in-depth information of physical properties of the population of NEOs between 50 and 300 m, in order to design mitigation missions and assess the consequences of an impact on Earth.

1. Introduction

The physical characterization of NEO surfaces is of fundamental importance, especially in view of the potential hazard some NEOs pose to human beings and more in general to life on our planet. Moreover, it allows us to put constraints on the material in the protoplanetary nebula at different solar distances, and can give us insights into the early processes that governed the formation and the evolution of planets, including the delivery of water and organics to Earth.

Unfortunately, our knowledge of the structure and composition of NEOs is still rather limited, since less than 15% of the known NEOs have physical properties determined from observations.

2. Observations and Discussions

In the framework of the EU project NEOShield-2, we will carry out these observations using guaranteed rapid access to Italian telescopes and facilities (e.g. Campo Imperatore, Asiago), as well as by competitive proposals to get access to medium/large and very large telescopes (e.g. TNG, LBT, and VLT). An operational interface will be maintained together with the ESA NEO Coordination Centre (NEOCC, http://neo.ssa.esa.int) in order to optimize observations devoted to physical characterization

The programme, status and goals, will be presented and discussed.

EPSC Abstracts
Vol. 10, EPSC2015-356, 2015
European Planetary Science Congress 2015

Photometric properties and variations across the surface of asteroid (21) Lutetia

N. Masoumzadeh (1), H. Boehnhardt (1), J. -Y., Li (2) and J. -B., Vincent (1)

(1) Max Planck Institute for Solar System Research, Justus-von-Liebig-Weg 3, 37077 Göttingen, Germany
(2) Planetary Science Institute, Tucson, AZ 85719, USA

Abstract

We applied the photometric functions of Minnaert and Hapke to multiband, visible-wavelength images of asteroid Lutetia, taken by OSIRIS (Optical, Spectroscopic, and Infrared Remote Imaging System) onboard the European Space Agency's Rosetta spacecraft during a close flyby in July 2010 [1, 2]. The modeled photometric parameters allowed to generate albedo ratio and phase ratio maps for an assessment of the overall light scattering behavior of Lutetia's surface. We also generated color ratio maps of Lutetia to fully investigate the photometric variations across the surface. Further interpretation of photometric parameters of Lutetia is done through the comparison with the available laboratory reflectance measurements and reflectance results for other small bodies in the solar system.

1. Introduction

Studying reflectance from the surface of asteroids and other atmosphereless small bodies provides information about optical properties and other physical properties of the regolith on the surface. Resolved images of the flyby at asteroid (21) Lutetia, returned by the OSIRIS imaging system onboard Rosetta spacecraft, enable us to study its surface reflectance.
In order to understand the surface evolution of Lutetia in the context of light scattering, we modeled the photometric parameters of the surface and scrutinized the photometric variations of regolith on Lutetia.

2. Photometric modelling

We employed two photometric models, i.e. that of Minnaert and of Hapke to model the disk-integrated and disk-resolved data of Lutetia in several filters. In order to extract the disk-resolved brightness, we developed a tool for extracting average intensity associated with geometric viewing angles per facet. The facet is the smallest element on the triangular shape model of Lutetia used in this analysis [3].
The two well-constrained multi-wavelength Hapke parameters of Lutetia are the single scattering albedo (SSA) and the roughness parameter. We calculate the spectral slope of the modeled SSA spectrum is estimated to be (1.65±0.29) % per 100 nm. We found that the best-fit value of roughness parameter of Lutetia ($\theta = 28^{\circ}$) does not vary significantly with the wavelength. The best-fit values of Hapke parameters at 649.2 nm of Lutetia (SSA= 0.226±0.002, B0=1.79±0.08, h=0.041±0.003, g=-0.28±0.01, θ=28°±1°) are similar to those of average S-type asteroids, particularly the single scattering albedo and the asymmetry factor g.
The modeled Minnaert k parameter of Lutetia at opposition (k_0=0.526±0.002) indicates a flat distribution in the surface brightness without significant limb darkening. No wavelength dependence is found for the Minnaert k value of Lutetia.

3. Comparison with laboratory reflectance measurement

In order to interpret the modeled Hapke parameters, we compare the disk-resolved data of Lutetia extracted from OSIRIS images at λ= 649.2 nm with the reflectance measurements from available terrestrial and extraterrestrial samples in the literature and found best-matches samples by Chromium oxide in the packed state [4] and an Allende meteorite sample [5].
We infer that the close similarity of these samples with the reflectance data of Lutetia is related to the consistency of the material, either by optical or structural properties or both.

4. Photometric variations

We generated albedo ratio maps (Figure 1) and phase ratio maps of Lutetia, using determined Minnaert parameters of the asteroid. The albedo variation on Lutetia is subtle (less than 10%) based on the albedo ratio maps of NAC F82 & F22 filter (649.2 nm) images at small phase angles ($\alpha < 30^{\circ}$). However, from the albedo ratio maps produced at large phase angle, a larger variation is noted for the so called NPCC region on Lutetia. The phase ratio maps of the asteroid do not display variation over the surface which may be caused by phase function or/and the photometric roughness alteration. This is confirmed by corresponding simulated phase ratio maps.

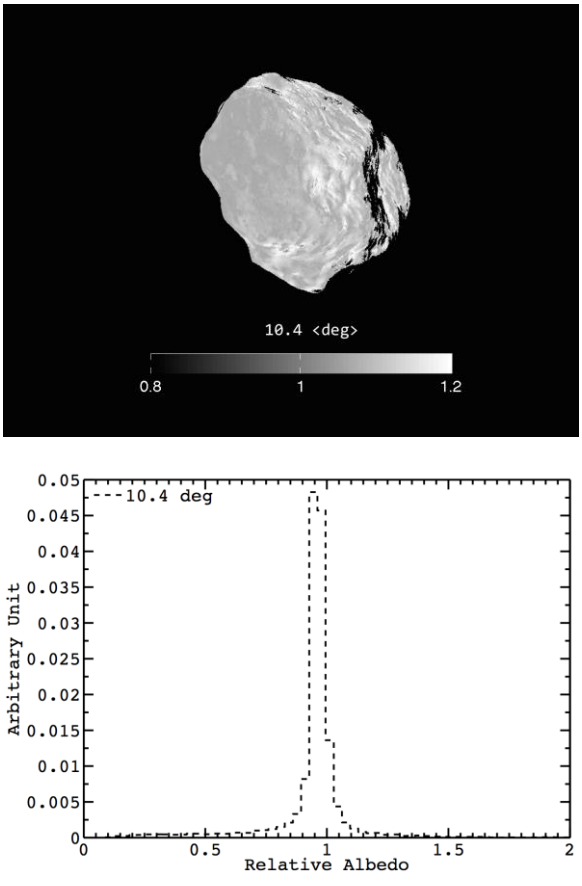

Figure 1: Upper panel displays the albedo ratio map of Lutetia from the NAC F82 image (λ =649.2 nm) at phase angle of 10.4°. Lower panel shows the corresponding weighted histogram of the albedo variations on Lutetia at α=10.4°.

Since the spectrum of Lutetia is featureless, we studied the variation of the spectral slope of Lutetia's spectrum across the surface. Color ratio map of the asteroid was produced using shape model registered images at 931.9-nm and 269.3-nm. The corresponding histogram of the color ratio map shows a symmetrical shape, indicating a rather uniform color variation across the surface. The FWHM of the distribution is 10%. In fact, on a large scale no obvious correlations between the color variations and the geological terrain on Lutetia were found. We note that on a smaller scale color variations are seen, for instance at the landslide location.

6. Summary and Conclusions

The uniform albedo and color contrast of Lutetia suggests two explanations; (a) the subsurface materials of Lutetia are similar to the regolith on surface at least for the reflectance of light, (b) the effect of space weathering is low for Lutetia and the surface is not altered displaying significant and large scale variations in its optical properties.

References

[1] Keller et al., OSIRIS – The Scientific Camera System Onboard Rosetta, Space Science Reviews, Vol. 128, pp. 433-506, 2007.

[2] Sierks, H. et al., Images of asteroid (21) Lutetia: A remnant planetesimal from the early solar system, Science, Vol. 334, pp. 487-490, 2011.

[3] Jorda, L. et al., Shape and physical properties of asteroid (21) Lutetia from OSIRIS images, in AAS/Division for Planetary Sciences Meeting Abstracts #42, 2010.

[4] Shepard, M.K. and Helfenstein, P., A test of the Hapke photometric model, Journal of Geophysical Research: Planets, Vol. 122, 2007.

[5] Beck, P. et al., Photometry of meteorites, Icarus, Vol. 228, pp.364 – 377, 2012.

EPSC Abstracts
Vol. 10, EPSC2015-358, 2015
European Planetary Science Congress 2015

Surface Exposure Ages of Space-Weathered Grains from Asteroid 25143 Itokawa

L. P. Keller (1), E. L. Berger (2) and R. Christoffersen (3)
(1) ARES, NASA Johnson Space Center, Texas, USA, (2) Geocontrol Systems – Jacobs JETS contract – NASA Johnson Space Center, Texas, USA, (3) Jacobs JETS contract – NASA Johnson Space Center, Texas, USA
(Lindsay.P.Keller@nasa.gov / Fax: +011-281-483-5374)

Abstract

We use the observed effects of solar wind ion irradiation and the accumulation of solar flare particle tracks recorded in Itokawa grains to constrain the rates of space weathering and yield information about regolith dynamics. The track densities are consistent with exposure at mm depths for 10^4-10^5 years. The solar wind damaged rims form on a much faster timescale, $<10^3$ years.

1. Introduction

Space weathering processes such as solar wind ion irradiation and micrometeorite impacts are widely known to alter the properties of regolith materials exposed on airless bodies. The rates of space weathering processes however, are poorly constrained for asteroid regoliths, with recent estimates ranging over many orders of magnitude [e.g., 1, 2]. The return of surface samples by JAXA's Hayabusa mission to asteroid 25143 Itokawa, and their laboratory analysis provides "ground truth" to anchor the timescales for space weathering processes on airless bodies.

1.1 Samples and Analysis Methods

Itokawa particles RAQD02-0211 (0211) and RA-QD02-0125 (0125) were allocated by JAXA; particle RA-QD02-0192 (0192) was allocated by NASA. Multiple electron transparent thin sections of each of these samples were prepared via a hybrid ultramicrotomy-focused ion beam (FIB) technique using an ultramicrotome and a FEI Quanta 3D dual-beam FIB-SEM [3]. Transmission electron microscope (TEM) analyses were acquired with a JEOL 2500SE 200kV field emission STEM.

2. Results

Itokawa particles 0211, 0192, and 0125 are olivine-rich (Fo_{70}) with minor Fe-sulfides. They have continuous solar wind damaged rims that are structurally disordered, nanocrystalline, and compositionally similar to the cores of the grains. All three particles have adhering mineral grains and melt particles, as well as solar flare particle tracks (tracks). Compared to lunar soil grains with a similar exposure history, the Itokawa grains are notable for a relative lack of abundant melt spherules and vapor deposits. Particle 0125 shows a track density of 9.8×10^8 tracks/cm^2) and a solar wind damaged rim thickness of ~50nm. Interestingly, the track densities and rim thicknesses vary across the other two particles. Particle 0211 exhibits a track density gradient across the grain that correlates with the rim thickness. The widest solar wind damaged rim (~80nm) is on the side of the particle with the highest track density (3.4×10^9 tracks/cm^2), while the thinnest rim (~40nm) is on the opposite side of the particle (track density: 9.2×10^8 tracks/cm^2). Particle 0192 also shows a track density gradient (2.9×10^9 to 1.1×10^9 tracks/cm^2) and has similar rim widths to particle 0211.

Solar flare energetic particles (mainly Fe-group nuclei) have a penetration depth of a few millimeters and leave trails of ionization damage in insulating materials that are readily observable by TEM imaging. The density of solar flare particle tracks is used to infer the length of time an object was at or near the regolith surface (i.e., its exposure age), but requires the accurate determination of a track production rate in order to convert track density into years of exposure. We used FIB-TEM techniques to obtain such a calibration using the track density/exposure age relations for lunar rock 64455. The 64455 sample was used earlier by [4] to

determine a track production rate by chemical etching of tracks in anorthite. Lunar rock 64455 had a stable orientation during its exposure on the lunar surface and displays a well-developed track density gradient in both anorthite and olivine. We measured a maximum track density at the sample surface of 8.2 $\pm 2.4 \times 10^{10}$ tracks/cm^2. Based on the measured track density and the Kr-Kr exposure age (2×10^6 y) for the splash glass on 64455 [4], we calculate a track production rate at 1 AU of $4.1 \pm 1.2 \times 10^4$ tracks/cm^2/y for a 2π exposure. Applying this track production rate to the Itokawa particles gives surface exposure ages of ~80,000 years for 0211, ~70,000 years for 0192, and ~24,000 years for 0125.

3. Discussion

Based on the solar flare particle track production rate in olivine at 1AU, the Itokawa grains recorded solar flare tracks over timescales of $<10^5$ years. Interestingly, the preservation of well-defined solar flare track gradients in two of the particles indicates that they maintained a relatively stable orientation at mm to cm depths for $\sim 10^4 - 10^5$ years in the Itokawa regolith. Plots of track density vs. depth for the two particles showing track gradients reveal no changes or breaks in slope suggesting the particles experienced little or no erosion of their surfaces.

Over timescales of a few 10^3 years, interaction with the solar wind produces ion-damaged rims on the outer ~100nm of grains that are exposed on the uppermost surface of lunar and asteroidal regoliths. The damaged rims on Itokawa grains are predicted to become amorphous and reach a steady state thickness of 80−100 nm within a few thousand years [5]. As the rims are not amorphous and portions are thinner than 60−70nm, this suggests their direct exposure to the sun was less than $\sim 10^3$ years. Although rims are generally continuous around the grain circumference, their thickness varies in a manner suggesting different sides of the grain had different solar wind exposure times. This indicates the Itokawa regolith was sufficiently dynamic for the grains to rotate, but no so dynamic that the grains become lost to space.

5. Summary and Conclusions

Space weathering of regolith particles on airless bodies results in a number of morphological changes, including cosmic ray exposure tracks, solar flare particle tracks and solar wind damaged rims. Each of these space weathering effects yields information about particle histories at different depths and over multiple timescales. Together, they give us information about the regolith dynamics on asteroid Itokawa. The heterogeneous distribution of the space weathering effects on two Itokawa particles is consistent with both particles maintaining a relatively fixed orientation in the Itokawa regolith throughout the time they were being irradiated by incoming solar flare ions. Solar flare particle tracks were formed over timescales of $10^4 - 10^5$ years, during which the Itokawa particles were shielded, at mm to cm depths, from direct exposure to the solar wind. The presence of track gradients in the particles indicates that the regolith in the Muses-C region on Itokawa was relatively stable at millimeter to centimeter-depths for the last $\sim 10^5$ years, implying little overturn. We conclude that only late in their history ($<10^3$ years) were the particles exposed to the solar wind. The continuous nature of the damaged rims on the Itokawa particles however, requires grain movement on the uppermost surface of Itokawa in order to expose all sides of the particles to the solar wind.

Acknowledgements

We thank JAXA and NASA for allocating particles for this study. This work was supported by a grant from the NASA Laboratory Analysis of Returned Samples program to LPK.

References

[1] Willman, M. et al.: Using the youngest asteroid clusters to constrain the space weathering and gardening rate on S-complex asteroids, Icarus, 208, 758-772, 2010.

[2] Vernazza, P. et al.: Solar wind as the origin of rapid reddening of asteroid surfaces, Nature, 458, 993-995, 2009.

[3] Berger, E. L. and Keller, L. P.: A hybrid ultramicrotomy-FIB technique for preparing serial electron transparent thin sections from particulate samples. Microscopy Today, 23, 18-22, 2015.

[4] Blanford, G. E., Fruland, R M. and Morrison, D. A.: Long-term differential energy spectrum for solar-flare iron-group particles, Proceedings of the Lunar and Planetary Science Conference, 6, 3557-3576, 1975.

[5] Christoffersen, R. and Keller, L. P.: Solar ion processing of Itokawa grains: Constraints on surface exposure times, Lunar and Planetary Science Conference, 46, #2084, 2015.

EPSC Abstracts
Vol. 10, EPSC2015-373, 2015
European Planetary Science Congress 2015

Survival of the impactor during hypervelocity collisions. An analogue for icy bodies.

Ch. Avdellidou (1), M.C. Price (1) and M.J. Cole (1)
(1) Centre for Astrophysics and Planetary Science, University of Kent, Canterbury, CT2 7NH, UK (ca332@kent.ac.uk)

Abstract

The majority of laboratory and simulation studies of hypervelocity impacts are dedicated to the investigation of the fate of the target bodies. However interest has increased in the fate of the projectile, as a result of several observational findings on asteroid surfaces, indicating the presence of material which does not match the overall lithology of the body. A possible explanation is that these materials are products of inter asteroid impacts in the Main Belt. Additionally, during the dynamical studies of asteroids collisions, the fate of the impactor was mainly neglected. We present the results of our laboratory programme devoted to measuring the survivability, fragmentation and state of the impactor, along with an estimation of the mass that was implanted on the target body, over a speed range of 0.38 - 3.5 km/s. Forsterite (Fo) projectiles were fired onto low porosity, water-ice targets, using the University of Kent's Light Gas Gun (LGG).

1 Introduction

Impacts have shaped asteroids, and their size frequency distribution, through 4.5Ga of Solar System evolution. The appearance and morphology of asteroidal surfaces are also the result of impact processes, which are responsible, for instance, for the formation of craters and the production of regolith. Over the last four decades, a plethora of laboratory experiments and computer simulations have provided insights into collision processes, but our understanding of the fate of the impactor at impact speeds of several km/s is still poorly understood. The fate of the projectile and projectile debris will potentially explain phenomena such as the source of the olivine and dark material deposits observed on Vesta [1] and the "Black Boulder" on (25143) Itokawa [2]. Asteroid 2008 TC3 consists of a peculiar case of a multi-lithology body whose origin is still unknown. A recent study [3] has shown that there is a little chance that foreign material remained on the surface of the body after low speed collisions with asteroids which orbits lay in a limited area in a-e space. There have been performed several laboratory experiments firing onto water-ice and regolith [4], studying the collision, as result from the aspect of the impactor. However, the collisional speed range that was tested was too low to simulate asteroid collisions. Considering an average impact speed of v = 5.3 km/s for Main Belt asteroid collisions [5], we show that material can be embedded on the target body at higher speeds.

2. Experiments

The gun used to perform these experiments is the horizontal two-stage LGG of the Impact Lab of the University of Kent. We used 3mm diameter Mg-rich peridots (Fo) as projectiles, fired with speeds 0.38-3.50 km/s onto low porosity (<10%) water-ice targets. As one of the aims of this project is to measure the size distributions of the projectile's fragments after the impact we built a set up with a water-ice layer to collect all the ejecta.

2.1 Fragment identification

After melting and filtering the ice from the target and the ejecta collecting set up, we ended up with filters that contain the projectile's fragments mixed with contaminating material from the gun. The majority of the contaminating material is C, Fe and Si. This led us to develop a different way to count and measure the olivine fragments. By using a Scanning Electron Microscope (SEM) and performing Energy-dispersive X-ray spectroscopy (EDX) we obtained raw images from scanning the filters that contained the projectile's fragments. Considering that (i) Fo projectiles have a very strong Mg signal and (ii) there is no Mg contamination from the gun, we used the EDX maps of Mg to identify the projectile fragments.

2.2 Photometry with Source Extractor

We applied a photometry technique to each image using the Source Extractor (SExtractor) open source software for astronomical photometry. SExtractor is able to extract every "light source" from the image and returns information about each source (such as the total number and the detected area of each fragment, major and minor axes, etc.).

3. Results

3.1 Size distribution of the ejecta

Following the procedures described above we constructed size frequency distributions for the range of speeds 0.92-3.50 km/s. The size frequencies follow log-normal distributions with a noticeable shift of the mode towards smaller sizes as the impact speed is increased.

3.2 Examination of the largest fragments

After each shot we collected the biggest fragment of the impactor found in the ejecta. The energy density at the time of the impact is Q [J/kg], and its general form is given by:

$$Q = \frac{1}{2}\frac{M_{im}}{M_t + M_{im}}v^2 \qquad (1)$$

where M_{im} is the mass of the impactor and M_t the mass of the target, and represents the kinetic energy of the impactor divided by the total mass of the system (see Fig. 1). Raman spectra were obtained of recovered fragments to ascertain whether the shock caused a shift in the olivine lines. Changes in the Raman spectra may also be indicative of changes to the crystallisation and/or the elemental composition of the olivine [6]. By comparing the spectra we collected before and after each shot we noticed a small shift of the two prominent olivine lines which increased with increasing collisional speed (approximate maximum shift 3 cm^{-1}). Additionally, simulations performed with AUTODYN hydro-code giving pressure and temperature values at the moment of the impact.

3.3 Contamination of the target

The general method we applied in order to estimate the mass of the impactor on the target filters is similar to the one described in §2. The goal was to calculate the volume of each fragment and derive its mass.

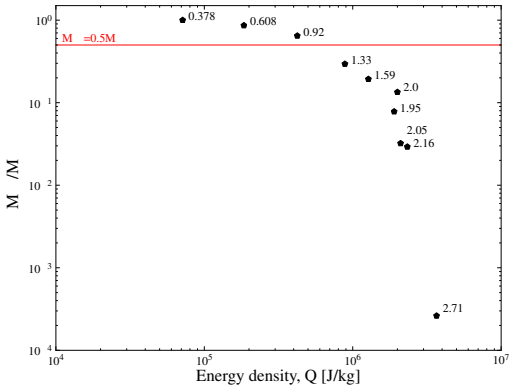

Figure 1: Mass ratio of the largest surviving fragment of the impactor versus the energy density Q_{im}. Catastrophic disruption occurred, when $M_{l,f}/M_{im}$=0.5 [numbers denote impact speed].

After having extracted the 2D area of each fragment, as projected on the detector, we had to estimate a z-axis that corresponds to the fragment's height. Tests were performed in order to show the randomness of the way that each fragment sits on the filter. By proving that there is not a preferable position of the fragments we were able to adopt simple estimations of the z-axis which had to follow similar distributions as x and y axes.

References

[1] V. Reddy et al. Delivery of dark material to Vesta via carbonaceous chondritic impacts. *Icarus*, 221:544–559, 2012.

[2] N. Hirata and M. Ishiguro. Properties and Possible Origin of Black Boulders on the Asteroid Itokawa. In *LPSC*, volume 42, page 1821, 2011.

[3] J. Gayon-Markt et al. On the origin of the Almahata Sitta meteorite and 2008 TC_3 asteroid. *MNRAS*, 424:508–518, 2012.

[4] H. Nagaoka et al. Degree of impactor fragmentation under collision with a regolith surface. Laboratory impact experiments of rock projectiles. *MAPS*, 49:69–79, 2014.

[5] W. F. Bottke et al. Velocity distributions among colliding asteroids. *Icarus*, 107:255–268, 1994.

[6] K. E. Kuebler et al. Extracting olivine (Fo Fa) compositions from Raman spectral peak positions. *GCA*, 70:6201–6222, 2006.

EPSC Abstracts
Vol. 10, EPSC2015-469, 2015
European Planetary Science Congress 2015

Asteroid polarimetry : validation run on the CAPS polarimeter

M. Devogèle (1,2), A. Cellino (3), G. Massone (3), S. Bagnulo (4), C. Pernechele (5), L. Abe (2), Ph. Bendjoya (2), C. Dimur (2), J.-P. Rivet (2), D. Vernet (2), O. Suarez (2)
(1) Institut d'Astrophysique et de Géophysique, Allée du 6 Août 17, Sart Tilman, Bât. B5c, 4000 Liège, Belgique, (2) Laboratoire Lagrange, UMR7293, UNS, CNRS, Observatoire de la Côte d'Azur, Nice, France, (3) INAF - Osservatorio Astrofisico di Torino, Pino Torinese 10025, Italy , (4) Armargh Observatory, College Hill, Armargh BT61 9DG, Northern Ireland, UK, (5) National Institute for Astrophysics, Astronomical Observatory of Padova, Italy. (Devogele@astro.ulg.ac.be)

Abstract

Polarimetric study of atmospherless bodies is a powerful tool to determine their physical properties (albedo, diameter) [1]. The "Calern Asteroids Polarimetric Survey" polarimeter has been designed for this purpose. It is a "single shot" CCD polarimeter based on a "double-Wollaston" configuration [3, 4]. This allows to measure simultaneously the three Stokes parameters *I*, *Q* and *U* without any moving parts. This instrument has been designed for the F/12.5 Cassegrain focus of the 1 meter West telescope of the "Centre Pédagogique Planète et Univers" facility (C2PU, Observatoire de la Côte d'Azur, Plateau de Calern, France). We present in this talk the first calibration and measurements made with CAPS. The results show that the instrument remained stable with a precision of 10^{-4} during the whole observing campaign (two months). We also present the very first polarimetric measurements on 30 main belt asteroids, in good agreement with previously published results.

1. Introduction

Usually, the degree of polarization for an asteroid is defined as the flux difference between the lights scattered with polarizations perpendicular and parallel to the scattering plane (normalized to their sum) :

$$P_{\mathrm{r}} = \frac{I_{\perp} - I_{\parallel}}{I_{\perp} + I_{\parallel}}. \qquad (1)$$

It is well known that the degree of polarization depends on the phase angle, *i.e.* on the angle between the Sun and the observer, as seen from the object.

For asteroids, the morphology of the "degree of polarization *vs* phase" curve $P_r = f(\alpha)$ has some general properties which are mainly dependent on their albedo. A feature common to all asteroids is a "negative polarization branch" for small phase angles (the polarization parallel to the scattering plane exceeds the polarization in the perpendicular direction). The transition from negative to positive polarization occurs for a critical value of the phase angle called the "inversion angle". For most asteroids this inversion angle has a relatively small value, around 20°.

The CAPS (Calern Asteroid Polarimetric Survey) is a new polarimeter dedicated to the observation of asteroids. This instrument aims at producing high quality "degree of polarization *vs* phase" curves for relatively bright asteroids (magnitude smaller than 16). One of CAPS major science case is to improve our knowledge about the relation between the polarization and the albedo [1]. In this context an interesting family of asteroids is the recently identified "Barbarian" family which display unusual polarimetric features [2].

2. Instrument description

The CAPS polarimeter is installed at the Cassegrain focus of the "Omicron" (West) telescope of the C2PU facility (Calern plateau, Observatoire de la Côte d'Azur, France; UAI code : 010). This telescope has an entrance pupil of 1.04 meter. For the Cassagrain focus, this leads to an aperture ratio of $F/12.5$. CAPS has been designed so as to allow simultaneous measurement of four polarization states (0°, 45°, 90°, and 135° *w.r.t.* the instrument's reference plane) on a single CCD frame. This is done by a double Wollaston prism [3, 4]. The common edge of those two Wollaston prisms subdivides an intermediate pupil image into two parts of equal surfaces. Each Wollaston prism splits the incoming light into two beams with complementary polarization states. The upper Wollaston prism separates polarizations 0° and 90°. The lower one separates polarizations 45° and 135°. Con-

sequently, four replicas of the same field of view are formed at the surface of the CCD sensor which correspond to the four polarization states.

3. Data reduction

After dark frame subtraction, a standard aperture photometry algorithm is applied separately to the four images of the same source. This yields the four polarized fluxes I_0, I_{90}, I_{45}, and I_{135} for the target. The Stokes parameters q and u are then computed according to their standard definitions :

$$q = \frac{I_0 - I_{90}}{I_0 + I_{90}}, \qquad u = \frac{I_{45} - I_{135}}{I_{45} + I_{135}} \tag{2}$$

Finally, the total polarization P and the polarization angle θ *w.r.t.* the instrument's reference direction are computed as follows :

$$P = \sqrt{q^2 + u^2}, \qquad \theta = \frac{1}{2} \arctan\left(\frac{q}{u}\right) \tag{3}$$

4. Observations

In the early 2015, a series of polarimetric standard calibration stars have been observed. These observations were used to calibrate the instrumental polarization and to measure the angular bias between the instrument's reference direction and the on-sky North direction (usually taken as the angular zero direction for on-sky polarization measurements). Repeating these observations on several polarimetric standard stars leads to an estimate of our measurements repeatability.

The optical components of the telescope and of the CAPS instrument are likely to introduce polarization biases. Those effects can be calibrated by the observation of a series of unpolarized standard stars. Since these stars are supposed to be unpolarized, any measured polarization is assumed to be due to these biases

The measurements on 17 unpolarized standard stars during 8 different nights shows a median instrumental polarization for the V band :

$$q_V(\%) = 3.82 \pm 0.018, \quad u_V(\%) = 0.27 \pm 0.007 \tag{4}$$

and for the R band :

$$q_R(\%) = 3.61 \pm 0.011, \quad u_R(\%) = 0.30 \pm 0.017 \tag{5}$$

where q and u are the reduced Stokes parameters (i.e. $q = Q/I$ and $u = U/I$).

The standard polarized stars are used to calibrate the angular bias between the instrument's zero direction and the on-sky North direction and to check if the instrumental component of the polarization are correctly subtracted. The measurements on 5 polarized standard stars during 5 different nights show that the CAPS instrument is rotated by $0.4^\circ \pm 0.4^\circ$ respectively with the IAU convention for the zero direction of polarization. The average difference between previously published polarization for these stars and the polarization found by CAPS after removing the instrumental component differ by $1.7 \times 10^{-4} \pm 2.7 \times 10^{-4}$

5. Results on asteroids

The CAPS instrument is dedicated to the observation of asteroids. Consequently, the full validation of the instrument requires observing asteroids for which the polarization *vs* phase relationship is well known. We have observed 30 asteroids during 8 nights. The results show that the polarization found is in agreement with the previously published measures.

6. Summary and Conclusions

The CAPS (Calern Asteroid Polarimetric Survey) instrument has been intensively tested during a two months validation run. The results show that the CAPS instrument provide reliable polarimetric measurements. In the meantime, the observation of standard polarimetric stars allowed us to test the instrument stabilibity, which is on the order of 10^{-4}.

Acknowledgements

Part of this work was supported by the COST Action MP1104 "Polarization as a tool to study the Solar System and beyond".

References

[1] Cellino, A. et al. "The strange polarimetric behavior of Asteroid (234) Barbara", Icarus, 180, 565, 2006

[2] Cellino, A. et al. "A new calibration of the albedo–polarization relation for the asteroids", JQSRT 113, 2552, 2012

[3] Oliva, E., "Wedged double Wollaston", a device for single shot polarimetric measurements", A&AS, 123, pp. 589- 592, 1997

[4] Pernechele, C. et al. "Device for optical linear polarization measurements with a single exposure", Proc. SPIE, 4843, 156-163, 2003

EPSC Abstracts
Vol. 10, EPSC2015-584, 2015
European Planetary Science Congress 2015

What we know about Oslo meteorite from cosmogenic isotope analysis

Z. Tymiński (1,2), M. Stolarz (1), T. Kubalczak (1), P. Zaręba (1), M. Burski, E. Mišta (2), K. Tymińska (2), E. Kołakowska (2), A. Burakowska (2), P. Żołądek (1), P. Saganowski (2), A. Listkowska (2), A. Olech (1,3) M. Wiśniewski (1,4)

(1) Polish Fireball Network, Comets and Meteors Workshop, ul. Bartycka 18, 00-716 Warsaw, Poland, (2) National Centre for Nuclear Research, ul. A. Soltana 7, 05-400 Otwock, Poland, (3) Copernicus Astronomical Center, Polish Academy of Sciences, ul. Bartycka 18, 00-716 Warsaw, Poland, (4) Central Office of Measures, ul. Elektoralna 2, 00-139 Warsaw, Poland

(z.tyminski@polatom.pl)

Abstract

The fragments of an asteroid that had crashed over Norway were found in a few locations in Oslo at the beginning of March 2012. Later on some pieces of meteorite from the most South area were collected by the Meteoritical Section members of Comet and Meteor Workshop (PKiM) with the help of local meteoritical authorities. One meteorite fragment of 32g was used to measure cosmogenic radionuclides using non-destructive high-resolution gamma spectrometry technique. Five radioisotopes such as Al-26, Na-22, Mn-54, Co-57 and Co-60 were detected.

1. Introduction

The Oslo meteorite which fall was not observed is still a puzzle. We collected information about the meteorite and analyzed the data to bring us closer to this unknown Norwegian phenomenon.

2. Meteorite finds

The first meteorite that had crashed through the roof of a cottage house was found in the central Oslo quarter Rodeløkka. Some days later the second discovery occurred in the melting snow of Ekebergsletta hilltop plateau. Pieces of the third meteorite, broken by cars and spread out by snowplow, were discovered on an asphalt road side by Maciek Burski, the member of Polish Meteoritical Society and by members of Meteoritical Section of PKiM. The last known pieces of the largest broken specimen were found in April 2012 in Grefsen approx. 2.5 km North from the cottage in Rodeløkka [1],[3],[4].

The total known mass of this unobserved fall of the ordinary chondrite (OC) is about 6.22 kg in five known findings spread out in the eight km-long N-S strewnfield with ~4.65kg and ~178g meteorites on the opposite ends. The list of meteorites with the location (listed from N to S) is shown in Table 1.

Table 1: List of known meteorite finds in Oslo

Location	Mass (g)	Notes
Grefsen	~4650	main mass ~3.5kg
Rodeløkka	~550	in 2 fit pieces
Ekeberg	~700+26	in 2 fit pieces
Frierveien - - kindergarten	178	many fragments
“Unknown”	115	complete stone
TOTAL :	~6219 g	

3. Measurements and analysis

Measurements and interpretation of gamma spectra were performed in the laboratories of National Centre for Nuclear Research suited in Otwock near Warsaw, in the Laboratory of Radioactivity Standards (RC POLATOM) and in the Laboratory of Environmental Analysis. The activity of samples was measured using a non-destructive method with the high resolution gamma ray spectrometers equipped with semi-conductor high purity germanium crystals cooled with LN_2 (-196^{o}C). The detectors with 20% - 45% relative efficiency and typical 2.0 keV energy resolution at 1332.5 keV have been used. To minimalize the background counting rate of measurements the detectors were enclosed in Pb-based shielding chambers. The acquisition system was realized by DSP analyzer connected to PC. The identification of radionuclides was obtained by analysis of spectra with GENIE-2K software. Detector efficiencies were calibrated for 1.0 ml vial by the series of radioactive solutions. To calculate the real efficiencies of the measurement geometries the

Monte Carlo methods were used. The corrections were obtained by PENELOPE and MCNP codes [2],[8]. The measurements of whole meteorite sample weighting 32g were carried out at distance of 1cm from detector top and acquisition time up to 200 hours [2],[8]. The list of isotopes usually detected in the meteorite samples is shown in Table 2. The analysis of the collected spectra does not indicate the presence of short live isotopes. Preliminary results of selected isotopes are presented on Fig.1 (on right).

Table 2: Isotopes expected in 32g Oslo sample

Isotope	Half-life	Detected
Cr-51	27.2 d	NO
Be-7	53.2 d	NO
Co-56	77.3 d	NO
Co-57	278.1 d	YES
Mn-51	312.1 d	YES
Na-22	2.60 y	YES
Co-60	5.21 y	YES
Al-26	7.2×10^5 y	YES

4. Summary and Conclusions

The studies of "fresh fallen" meteorites show that the content of Be-7 always reaches quite high value [2],[5],[6],[7]. Since we could not get the signal from this isotope we can conclude that it had decayed to a level undetectable by the techniques used. Assuming its highest "invisible" final content it can be possible to estimate the approximate minimal terrestrial age of the meteorite. The analysis are presented in Figure 1. where the extrapolation of specific radioactivity level for selected isotopes is shown for two meteorites: Oslo and Ghopij L3-5 breccia. We chose Ghopij breccia chondrite for comparison because Oslo meteorite is very similar to OC type breccia [1]. The comparisons started with the Be-7 MDA (Minimal Detectable Activity) value calculated as ~3 dpm/kg (decays/ minute/ kg) for Oslo. Tracking back in time the activity to the observed minimal value of Be-7 as measured in Ghopij chondrite we obtained the period of 170 days. The estimates calculated with the contents of other isotopes observed in Oslo (Fig.1) confirm the corresponding isotopes concentrations in Ghopij. The content of Mn-54 and within the limits of uncertainty, the level of Co-57, fit to the proposed terrestrial age of about 3 half-lives of Be-7. On the other hand the result of Na-22 calculation shows to low concentration in Oslo comparing to Ghopij. This may indicate the several months stay on Earth or very low initial Na-22 concentrations in Oslo meteorite.

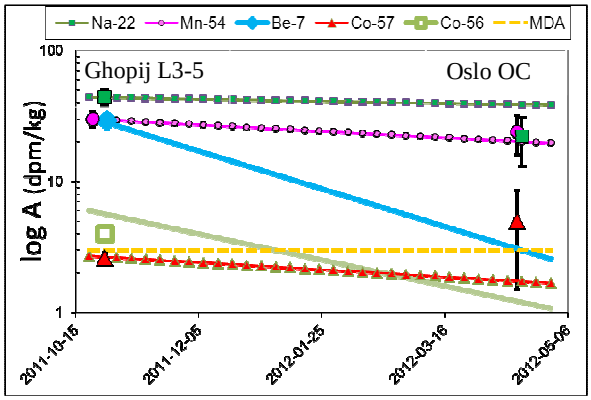

Figure 1: Extrapolation of logarithm radionuclide activity (log A) change in time in Oslo and Ghopij meteorites for selected isotopes based on the decay law. The preliminary results obtained for Oslo are presented on right (ref. date 15.04.2012) and for Ghopij L3-6 on left-side (ref. date = time of fall) [5]. Dashed orange line presents the MDA - Minimal Detectable Activity, the minimum threshold of Be-7 detection in measurement conditions.

Acknowledgements

This work was supported by NCN grant number 2013/09/B/ST9/02168 to A. Olech.

References

[1] Tymiński Z., et.al.: Search report of meteorites in Oslo, Acta Soc. Metheor. Pol., vol.4, pp. 108-114, 2013.

[2] Tymiński Z., et.al.: The Oslo meteorite research for cosmogenic radionuclides and the interpretation of the results, Acta Soc. Metheor. Pol., vol.4, pp. 115-120, 2013.

[3] Bilet M.: Oslo-Meteoritten, Astronomi, No. 4 Årg. 42, pp.10 – 13, 2012.

[4] Burski M.: Oslo, marzec 2012, Meteoryt No. 1 (81), pp.27 – 28, 2012.

[5] Bhandari N., et al.: Itawa Bhopji (L3-5) chondrite regolith breccia: Fall, classification, and cosmogenic records. MAPS, vol. 37, pp. 549–563, 2002.

[6] Leya I., Masarik J.: Cosmogenic nuclides in stony meteorites revisited. Meteoritics & Planetary Science, vol. 44, pp.1061–1086, 2009.

[7] Evans J. C., et.al.: Cosmogenic nuclides in recently fallen meteorites: Evidence for galactic cosmic ray variations during the period 1967-1978. Journal of Geophysical Research, vol. 87, pp. 5577–5591, 1982.

[8] Tymiński Z., et.al.: Samples at gamma spectrometry laboratory, Proceedings of the IMC, vol. 2, pp. 193, 2014

EPSC Abstracts
Vol. 10, EPSC2015-593, 2015
European Planetary Science Congress 2015

An efficient algorithm for prioritizing NEA physical observations

M. Cortese (1,2), **E. Perozzi** (2,3,5), B. Borgia (3,6), M. Micheli (3,5,6), G. D'Abramo (5), E. Dotto (4), E. Mazzotta Epifani (4), S. Ieva (4), M.A. Barucci (7), D. Perna (7).
(1) Dip. di Matematica, Universita' di Roma Tor Vergata, Italy, (2) Deimos Space, Romania, (3) ESA-NEOCC, Italy, (4) INAF-Osservatorio Astronomico di Roma, Italy, (5) INAF-IAPS Roma, Italy, (6) SpaceDyS, Italy, (7) LESIA- Observatoire de Paris, France

Abstract

The present NEA discovery rate has overcome 1500 objects per year thus calling for extensive observation campaigns devoted to physical characterization. A tool is presented which, through a prioritization algorithm, aims to optimize the planning and the execution of NEA physical observations.

1. Introduction

The problem of efficiently planning and executing NEO follow-up observations has been originally addressed by the Spaceguard Central Node to ensure that the highest possible percentage of these objects, and in particular the newly discovered ones, is recovered at other apparitions. Therefore a prioritization algorithm, which ranks the observable objects according to an urgency criterion, was developed [1]; since more than 10 years it produces a list of targets needing astrometric observations ranked in term of urgency. These lists are publicly available at the Spaceguard Central Node and at the ESA NEO Coordination Centre web sites. In the present work a similar approach has been followed for addressing the prioritization of NEA physical observations.

2. Prioritization algorithm

The prioritization algorithm has been substantially revised in order to account for the technical requirements of the NEOShield-2 project [2] (recently approved by the European Commission in the framework of the Horizon 2020 programme), i.e. increase the number of NEAs for which physical characterization is available by focusing on objects in the 50-300 m size range and which are potentially accessible for a space mission.

Various parameters have been taken into account: the sky uncertainty, the visibility period, the phase range, an estimate of the object apparent motion and of its accessibility (provided by a best-case transfer strategy). Two ranking criteria are introduced, "urgency" and "importance", which correspond to different observing scenarios. The former is a function of the number of visibility days and of the magnitude trend and applies especially for newly discovered objects at risk of being again observable only after a long time span, thus calling for rapid response times. The latter is a function of the object size and accessibility, providing the rationale for planning large observing programs.

3. Figures

The dimension function (DIM) used in the "importance" ranking computation is modeled as shown in Figure 1. It is closely related to the absolute magnitude of the object [3].

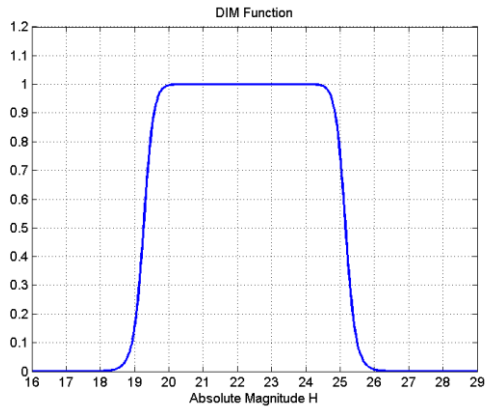

Figure 1: DIM function used in the "importance" ranking computation.

6. Summary and Conclusions

The prioritization of NEA follow-up observations has been extended to physical characterization. The resulting tool will generate a daily table of observable targets and it can be also run as a stand-alone tool in order to provide future observing opportunities at a specific date of interest. It is planned to make these data publicly available through the NEOShield-2 web site.

References

[1] Boattini A., D'Abramo G., Valsecchi G.B., and Carusi A.: A New Protocol for the Astrometric Follow-up of Near Earth Asteroids, Earth, Moon and Planets, Vol. 100, pp. 31-41, 2007.

[2] NEOShileld-2: Science and Technology for Near-Earth Object Impact Prevention. EU Horizon 2020 Programme PROTEC-2, 2014.

[3] Chesley S.R., Chodas P.W., Milani A, Valsecchi G.B., and Yeomans D.K.: Quantifying the Risk Posed by Potential Earth Impacts, Icarus, Vol. 159, pp. 423-432, 2002.

EPSC Abstracts
Vol. 10, EPSC2015-643, 2015
European Planetary Science Congress 2015

Terrestrial planet formation constrained by the structure of the asteroid belt

Andre Izidoro (1), Sean N. Raymond (2) , Alessandro Morbidelli (3) and Othon C. Winter (4),
(1) Université de Bordeaux, Laboratoire d'Astrophysique de Bordeaux, Floirac, France. (izidoro.costa@gmail.com)
(2) CNRS, Université de Bordeaux, Laboratoire d'Astrophysique de Bordeaux, Floirac, France.
(3) CNRS, Université de Nice-Sophia Antipolis, Observatoire de la Côte D'Azur, Nice, France.
(4) Unesp, Univ. Estadual Paulista, Grupo de Dinâmica Orbital e Planetologia, Guaratinguetá, São Paulo, Brazil

Abstract

Reproducing the large mass ratio between the Earth and Mars requires that the protoplanetary disk had a strong mass depletion in solids between roughly 1 AU and 3 AU. The Grand Tack model invokes a specific migration history of the giant planets of the Solar System to remove most of the mass initially beyond 1 AU and to leave the asteroid belt on an excited dynamical state. However, one could also invoke that a steep density gradient was created by the inward drift and pile-up of a large amount of small particles induced by gas-drag. Using a series of N-body numerical simulations in disks with steep surface density profiles we show that that disks with shallow density gradients reproduce the dynamical excitation of the asteroid belt by gravitational self-stirring, but inevitably form Mars analogs that are significantly more massive than the real planet. In contrast, a disk with a surface density gradient proportional to $r^{-5.5}$ beyond 1 AU reproduces the Earth/Mars mass ratio but leaves the asteroid belt in a dynamical state that is far colder than the real belt. We conclude that a steep mass distribution in the protoplanetary disk cannot produce the inner solar system. Thus, the asteroid belt has to have been depleted and dynamically excited by an external agent as, for instance, in the Grand Tack scenario.

1. Introduction

In classical numerical simulations, the assembly of the terrestrial planets is simulated from the accretion of Moon-mass to Mars-mass planetary embryos and smaller planetesimals orbiting between ∼0.5 and ∼4 AU [1]. This scenario has been proven successful in producing a variety of constraints as for example: Earth and Venus analogs, accounting for the origin of Earth's water and its accretion within the timescale consistent with radioactive chronometers [2]. Despite these appealing achievements, classical simulations also suffer from some important drawbacks. One of the most important ones is that the planet formed around 1.5 AU is about 5-10 time more massive than the real planet in these simulations [3]. One solution to the so-called "Mars problem" is to invoke that the terrestrial planets formed from a narrow annulus, with a steep mass density gradient beyond 1 AU [4].

The Grand Tack model [5] invokes a specific migration history of Jupiter and Saturn during the gas-disk phase to remove most of the mass initially beyond 1 AU, creating a narrow annulus of mass around 1 AU, and to leave the asteroid belt on an excited dynamical state. An alternative to the Grand Tack scenario to produce the confined disk and a mass deficient asteroid belt could be invoke that a lot of solid material drifted to within 1 AU by gas drag, leaving the region beyond 1 AU substantially depleted in mass. This idea is very appealing in a broad context of planet formation. This is because it is often invoked to produce a large pile-up of mass in the inner disk to explain the formation of close-in super-Earths (eg. [6-7]). Therefore, the goal of this paper is to test whether any of these gradients could explain at the same time the small mass of Mars and the properties of the asteroid belt (mass deficit and inclination excitation).

2. Methods

The simulations presented in this paper fit in the context of the classical scenario of terrestrial planet formation. We perform simulations starting from disks with a wide range of surface density profiles. We tested disks with surface density profiles given by $\Sigma_1 r^{-x}$, where x = 2.5, 3.5, 4.5 or 5.5 and r is the heliocentric distance. Σ_1 is the solid surface density at 1 AU. Our disks extends from 0.7 to 4 AU. We adjusted Σ_1 to fix the total mass in the disk between 0.7 and 4 AU at $2.5 M_\oplus$, comparable to the sum of the masses of the

terrestrial planets. Our simulations also included fully-formed Jupiter and Saturn on orbits consistent with the latest version of the Nice Model [8]. During our simulations, we neglect gas drag and gas-induced migration of the planetary embryos.

3. Results

Our results show that steeper disks (higher x) produce smaller planets around 1.5 AU. This is to be expected since steeper disks have less mass in their outer parts (for a fixed disk mass). Therefore, they are closer to the idealized initial conditions proposed by [4], namely a disk truncated at 1 AU. The simulations with x of 2.5, 3.5 and 4.5 do not reproduce the terrestrial planets because they produce planets at around 1.5 AU that are systematically too massive compared to Mars. Only our steepest disk profiles (x = 5.5) produced good Mars analogs, but those simulations yielded an under-excited asteroid belt. Simulations with flatter disk profiles formed Mars analogs far more massive than the actual planet. Those simulations excited the asteroid belt to roughly the right amount but failed to adequately match observations because too many embryos were stranded in the belt, for example.

4. Conclusions

Using a series of simulations of terrestrial planet formation in disks with steep surface density profiles we show that the asteroid belt orbital excitation provides a crucial constraint against the inward migration and pile up pf small particles induced by gas-drag, for the solar system. Simulations with a surface density gradient proportional to $r^{-5.5}$ can indeed to reproduce the Earth/Mars mass ratio, but leaves the asteroid belt on a dynamical state way too cold compared to the real belt. In contrast, shallow density gradients allow the dynamical excitation of the asteroid belt by a self-stirring process, but lead inevitably to the formation of a Mars analog which is significantly more massive than the real planet.

We find the small mass of Mars and the dynamical excitation of the asteroid belt have diametrically opposite scalings; Mars' small mass requires a mass deficit but producing asteroids with inclinations above ~ 10 degrees requires a significant amount of mass in embryos. Therefore, we conclude that no disk profile can explain at the same time the structure of the terrestrial planet system and of the asteroid belt. Thus, the asteroid belt has to have been depleted and dynamically excited by an external agent as, for instance, in the Grand Tack scenario.

Acknowledgements

A. I, A. M. and S. R thank the Agence Nationale pour la Recherche for support via grant ANR-13-BS05-0003-01 (project MOJO). A. I. also thanks partial financial support from CAPES Foundation (Grant: 18489-12-5). O. C. W thank support financial support from FAPESP (proc. 2011/08171-03) and CNPq.

References

[1] Chambers, J. E.: Making More Terrestrial Planets, Icarus, v. 152, p. 205, 2001

[2] Raymond, S. N., O'Brien, D. P., Morbidelli, A., & Kaib, N. A.: Building the Terrestrial Planets: Constrained Accretion in the Inner Solar System, Icarus, v. 203, p. 644, 2009

[3] Izidoro, A., Haghighipour, N., Winter, O. C., & Tsuchida, M.: Terrestrial Planet Formation in a protoplanetary disk with a local mass depletion: A successful scenario for the formation of Mars, The Astrophysical Journal, v. 782, p. 31, 2014

[4] Hansen B.: Formation of the Terrestrial Planets from a Narrow Annulus 2009, The Astrophysical Journal, v. 703, p. 1131, 2009

[5] Walsh, K. J., Morbidelli, A., Raymond, S. N., O'Brien, D. P., & Mandell, A. M.: A low mass for Mars from Jupiter's early gas-driven migration, Nature, v. 475, p. 206, 2011

[6] Boley, A. C., & Ford, E. B.: The Formation of Systems with Tightly-packed Inner Planets (STIPs) via Aerodynamic Drift , arXiv:1306.0566

[7] Chatterjee, S., & Tan, J. C.: Inside-out Planet Formation, The Astrophysical Journal, v. 780, p. 53, 2014

[8] Levison, H. F., Morbidelli, A., Tsiganis, K., Nesvorný, D., & Gomes, R.: Late Orbital Instabilities in the Outer Planets Induced by Interaction with a Self-gravitating Planetesimal Disk, Astronomical Journal, v. 142, p. 152, 2011

EPSC Abstracts
Vol. 10, EPSC2015-648, 2015
European Planetary Science Congress 2015

V-type asteroids: a tale of two parent bodies?

S. Ieva (1), E. Dotto (1), D. Perna (2), D. Fulvio (3), D. Lazzaro (4) and M. Fulchignoni (2)

(1) INAF – Osservatorio astronomico di Roma, Italy (2) LESIA – Observatoire de Paris, France, (3) Laboratory Astrophysics Group of the Max Planck Institute for Astronomy, Germany (4) Observatorio Nacional, MCT, Brasil (simone.ieva@oa-roma.inaf.it)

Abstract

The majority of basaltic V-type objects, found in the inner main belt, are dynamically linked to the asteroid Vesta, the only large basaltic differentiated object in the main belt. The discovery of small basaltic objects in the middle/outer main belt (MOVs) not dynamically linked to Vesta points out that Vesta could not be the parent body for all the basaltic objects in the Solar System.
We performed an improved statistical analysis using several spectral parameters in the visible, near-infrared and VNIR range in order to assess similarities and differences in the surface composition of Vesta family objects and other V-type asteroids. Our results strongly suggest that MOVs do not have an origin compatible with Vesta.

1. Introduction

In the last decades several main belt asteroids have been found showing a basaltic composition, similar to those of Vesta and basaltic HED achondrite meteorites. The majority of these objects, classified as V-type according the most recent taxonomy [1], are thought to be originated from a huge collisional event on the south pole of Vesta [2], and show orbital parameters (a,e,i) close to Vesta itself.
V-type asteroids were also found outside the boundaries of the dynamical family: while at least one group could be considered as *"fugitives"* [3] from the Vesta family through resonant and/or non-gravitational effects, it is difficult to explain other V-types not dynamically linked to Vesta. Some of them reside on the other side of the 3:1 mean motion resonance with Jupiter [4,5] and, according to the current dynamical models, it would be very unlikely that a fragment survived through the passage of such a powerful resonance.

The classical scenario suggested that in the early Solar System only Vesta has achieved the size and conditions to retain large amounts of radioactive elements, in order to produce the necessary heat to melt the original chondritic material and form a core, a mantle and a basaltic crust. Recent laboratory studies on meteorites [6] has proven that at least five other large asteroids (D > 150 - 300 km) in the main belt should have undertake a complete differentiation. These elusive basaltic bodies, probably "battered to bits" in the early phases of our Solar System, could be the parent bodies of basaltic asteroids not dynamically linked to Vesta; or our understanding of differentiation processes in the early Solar System could be incomplete [7].

2. Results

In order to highlight similarities and differences in the surface composition of V-types, belonging and not belonging to the Vesta dynamical family, we performed a statistical analysis on spectral parameters (reflectivity gradients, band centres, band separation) computed for 115 V-type asteroids. We divided our sample in six dynamical classes: vestoids (or Vesta family), fugitives, low-inclination, Inner Other (IOs), V-type NEAs and Middle/Outer V-types (MOVs). We also compared our sample with HED meteorites spectra taken from the RELAB database [8] and spectra of the surface of Vesta taken by the VIR spectrometer on board of the Dawn mission [9].
Our analysis has proven that while V-type dynamical classes in the inner main belt (Vesta family, fugitives, low-inclination, IOs) show compatible spectral parameters, this seems not to be the case for V-type NEAs and MOVs. The extreme variation of spectral properties found on NEAs could be due to a balance between space weathering processes and a rejuvenation of surfaces, although a different origin could not be excluded. MOVs show spectral parameters, location in the main belt and sizes

incompatible with Vesta, strongly pointing towards an origin from a different basaltic parent body.

References

[1] DeMeo, F. E., Binzel, R. P., Slivan, S. M. et al. 2009, Icarus, 202, 160

[2] Marchi, S., McSween, H. Y., O'Brien, D. P. et al. 2012, Science, 336, 690

[3] Nesvorny, D., Roig, F., Gladman, B. et al. 2008, Icarus, 193, 85

[4] Lazzaro, D. Michtchenko, T., Carvano, J. M. et al. 2000, Science, 288, 2030

[5] Binzel, R. P., Masi, G., Foglia, S. 2006, BAAS, 38, 627

[6] Scott, E., Greenwood, R., Franchi, I. et al. 2009, GeCoA 73, 19

[7] Weiss, B. & Elkins-Tanton, L. 2013, AREPS 41, 529

[8]http://www.planetary.brown.edu/relabdocs/relab_disclaimer.htm

[9] De Sanctis, M. C., Coradini, A., Ammannito, E. et al. 2011, SSRv, 163, 329

EPSC Abstracts
Vol. 10, EPSC2015-651, 2015
European Planetary Science Congress 2015

Evolution of Zakłodzie enstatite meteorite – insight from TEM analyses

A. Krzesińska (1), R. Wirth (2) and M.A. Kusiak (3)
(1) Institute of Geological Sciences PAS, ING PAN Wrocław, Poland, (agatakrz@twarda.pan.pl), (2) Geoforschung Helmholtz Zentrum, Potsdam, Germany, (3) Institute of Geological Sciences PAS, ING PAN, Warsaw, Poland.

1. Introduction

The Zakłodzie meteorite is an achondritic-like rock with enstatite chondrite parentage [1,2,3]. Its texture indicative for complicated thermal history and various processes were proposed to account for this [1,2,3]. Based on the mineral composition it was concluded that the rock represents EL7 enstatite chondrite [1]. Twinned enstatite and zonal feldspar crystals in Zakłodzie were interpreted as formed by impact melting and rapid crystallization [2]. On the other hand, cumulate structure was considered to result from igneous processes and slow cooling of the meteorite [3]. The aim of presented study was to define whether Zakłodzie formed by shock event on chondritic parent body or by slow cooling from high temperatures typical for achondritic meteorites.

2. Samples and methods

The FIB-TEM measurements were performed on twinned pyroxene crystals from achondritic-like Zakłodzie meteorite. Several striated low-Ca pyroxene crystals were examined by Tecnai F20x-twin transmission electron microscope in GFZ, with a field emission gun electron source, operating at 200 kV.

3. Results

Analysis of thin foils reveals that the pyroxene has striated structure and consists of disordered mixture of both orthorhombic and monoclinic polymorphs. In high resolution images (Fig. 1) the polymorphs are heterogeneously distributed. Domains of monoclinic pyroxene are relatively broad (up to 40 nm in size i.e., they consist of more than 40 unit cells of cpx). The thickness of cpx domains is highly heterogeneous, and in some parts very thin lamella of cpx overgrown with opx are also abundant. Orthorhombic polymorph of pyroxene is minor. It forms usually very thin lamella, only limited number of lamella up to 20 nm in width was observed.

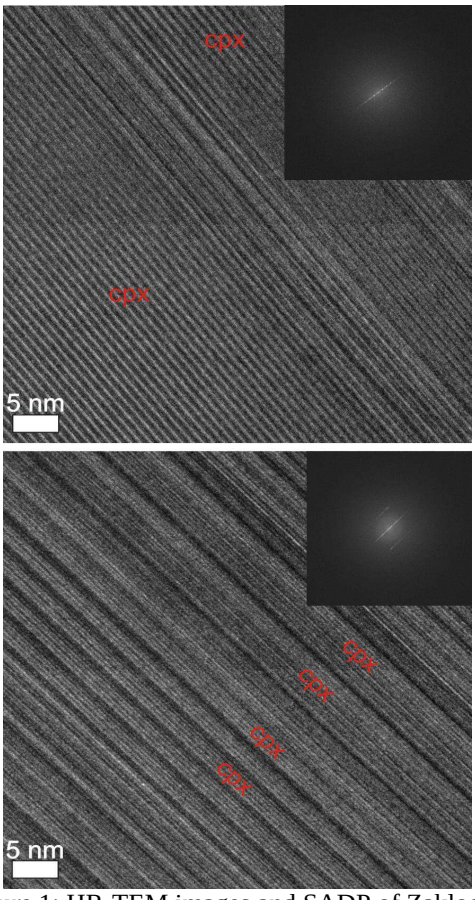

Figure 1: HR-TEM images and SADP of Zakłodzie meteorite showing high heterogeneity of clinopyroxene (cpx) and orthopyroxene (opx) distribution with dominance of cpx.

Electron diffraction patterns (Fig. 1) show strong streaking, confirming high degree of disorder of pyroxene. Streaking observed in diffraction patterns is most probably the result of the stacking disorder

produced by the coherent interleaving of blocks of ortho- and clinoenstatite. However, strong diffraction maxima at 9Å are observed, characteristic of the domination of clinopyroxene (Fig. 1).
In regions of strong striation, pyroxene reveals additional diffraction contrast, manifesting in presence of short, up to 200 nm, domains located along individual lamella (Fig. 2a). Presence of such heterogeneously distributed domains is interpreted here as a result of kinking.

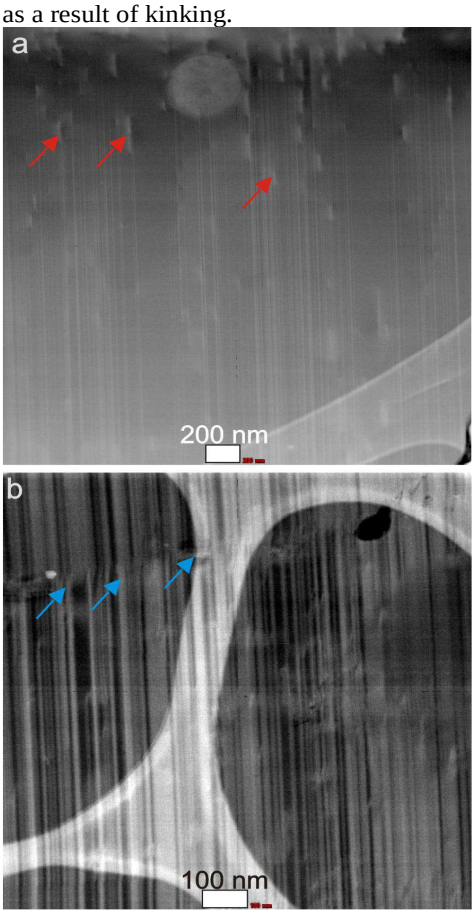

Figure 2: STEM images of Zakłodzie meteorite. a. Kinked lamella of pyroxene. b. Annealed crack.

In spite of being sheared and kinked, lamella are also cracked. In many cracks, traces of recrystallization and annealing are observed (Fig. 2b).

4. Discussion

Intergrowths of ortho- and clino- polymorphs of pyroxene can develop by a number of different mechanisms. They may form in response to high-temperature inversion from protoenstatite during cooling [4,5] or may result from annealing of clinopyroxene within orthopyroxene stability field, or in opposite conditions [4]. Additionally, intergrowths may form in sustained shearing, either homogeneous or heterogeneous (i.e., shock-related) [6].
Nanostructure of the rock-forming pyroxene in Zakłodzie i.e., heterogeneous distribution of orthorombic and monoclinic polymorhps, domination of clinopyroxene and large thickness of its domains (Fig. 1) are suggestive of pyroxene inversion due to shearing and shock [6]. Kinking of lamella (Fig. 2a) is in good agreement with such model of formation. Thus, the results suggest that Zakłodzie meteorite experienced severe shock event on the parent body, which was main event in its evolution. However, shock event itself is not sufficient to cause strong annealing observed in pyroxene of Zakłodzie (Fig. 2b). We suggest that after the shock event, the meteorite was buried in deep part of warm ejecta and thermally annealed. The temperatures attained for pyroxene annealing might have been sufficient to cause partial melting of plagioclase, observed in meteorite by [2,3]. Presented results demonstrate that the Zakłodzie meteorite is most probably genetically related to enstatite chondrites rather than to aubrites or primitive achondrites, despite of its achondritic-like texture.

Acknowledgements

The research was conducted thanks to funding from 7th Framework Programme, RegPot (ATLAB 285989).

References

[1] Stępniewski M., et al. 2000.: Preliminary study of a new enstatite meteorite form Zakłodzie (southeast Poland). Met. and Planet. Sci. 35: A152–A153.

[2] Keil K. 2010: Enstatite achondrite meteorites (aubrites) and the histories of their asteroidal parent bodies. Chemie der Erde 70: 295–310.

[3] Przylibski T.A. et al. 2005.: The Zakłodzie enstatite meteorite: Mineralogy, petrology, origin, and classification. Met. and Planet. Sci. 40: A185–A200.

[4] Buseck P.R., et al. 1982: Subsolidus phenomena in pyroxenes. Rev. Mineral. 7: 117–211.

[5] Jones R.H. and Brearley A.J. 1992: An experimental and TEM investigation of the effects of cooling rate on the proto-to-ortho transition in enstatite. EOS-Trans. Amer. Geophys. Union 73: 619.

[6] McCoy T.J., et al. 1995. Origin and history of impact-melt rocks of enstatite chondrite parentage. Geoch. Cosmoch. Acta 59: 161–175.

EPSC Abstracts
Vol. 10, EPSC2015-796, 2015
European Planetary Science Congress 2015

Tidal Disruption of Phobos as Cause of Surface Fractures

E. Asphaug[1], T. Hurford[2], J.N. Spitale[3], D. Hemingway[4], A. R. Rhoden[1,5], W. G. Henning[2,6], B. G. Bills[7] and M. Walker[8]
[1]Arizona State University, Tempe AZ; [2]NASA Goddard Space Flight Center, Greenbelt MD; [3]Planetary Science Institute, Tucson AZ; [4]UCSC, Santa Cruz CA; [5]Johns Hopkins Applied Physics Laboratory, Laurel MD; [6]U. Maryland, College Park MD; [6]JPL, Pasadena CA; [7]UCLA, Los Angeles CA. Contact email: easphaug@asu.edu

Abstract

Phobos displays an extensive system of grooves that are mostly symmetric about its sub-Mars point. The ~20 km diameter satellite is spiraling in due to the tides it raises. It will undergo tidal disruption [1, 2] before crashing into Mars in tens of millions of years [3]. We compute the tidal evolution of the de-orbiting satellite and show that most of its prominent grooves have excellent correlation with the resulting stress in a thin elastic shell. The model requires a very weak interior (rubble pile) overlain by a somewhat cohesive exterior (~1 MPa), similar to interpretations [4] of comet 67P/C-G and consistent with the predicted behavior of microgravity regolith [5, 6, 7].

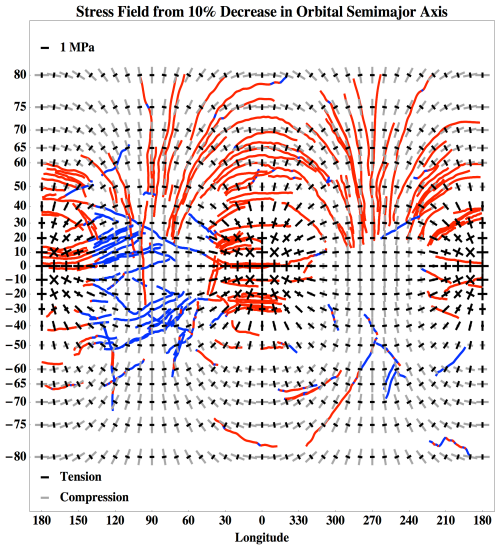

Figure 1. Stresses in a 10 m elastic shell computed for the last 10% of orbital decay (Fig. 2) for a spherical Phobos with much weaker interior. Stresses are in tension radial to the tidal bulge (0° and 180°) and in compression concentric to it; both axes are in tension near the bulge. Most observed grooves experience tensile stress across their strike (red); anomalous grooves (blue; mostly in leading hemisphere) require a different mode or time of origin.

Methods

Shortly after Viking obtained the first geomorphic images of Phobos, it was proposed [8] that stresses from orbital decay cause grooves. The idea proved unworkable in the context of a homogeneous spheroid. We apply a two-layer stress model [9] with ρ_{av}=1.88 g/cm^3, inner rigidity μ=10^6 Pa, and outer rigidity μ=10^{10} Pa in a 10 m thick shell. As the satellite de-orbits, the tidal deformation increases, resulting in a growing surface stress that we compute using a spherical thin shell approximation [10, 11].

We then mapped ~200 of the most prominent linear features on Phobos. Using the latitude, longitude and strike for multiple points along these fractures, we calculated: the principal tidal stress experienced along their tracks, the orbital decay stress parallel and perpendicular to each fracture, and the shear stress across each fracture. The magnitudes of the computed stresses, and the correlation between principal stress orientations and the azimuths of observed fractures, provide the critical tests of the tidal fracturing model.

For a range of parameters where a weak Phobos is overlain by a more rigid surface layer, we obtain (Figure 1) a strong correlation between the surface stress field due to orbital decay and the geometry of grooves. Orbital decay from 3.04 to 2.77 R_{mars} can produce >1 MPa of surface tensile stress (Figure 2). The majority of grooves (red) align with the local tensile stress, indicating that they could have formed (or are forming) by tensile failure of the surface.

Tidally-aligned grooves are absent S/SE of the sub-Mars point. This might be attributed to the absence of a cohesive surface layer in this location (nothing to record the strain), or to structural collapse or impact reverberation. In our model, fracture walls are weak (~1 MPa) and only strong in comparison to the rubble pile interior. Non-aligned grooves (blue) require an alternative explanation. They could have formed earlier when Phobos was in a different tidally

locked orientation [12]. The are found predominately in the leading hemisphere, perhaps consistent with the idea that Phobos swept up co-orbiting debris [e.g., 13]. By quantifying the grooves according to their goodness of fit to the tidal stress, we set the stage for comparative geomorphic analysis, that awaits higher definition imaging of Phobos.

A weak interior with an elastic shell is more commonly associated with terrestrial planets and icy moons than with small bodies. But another such body is the Jupiter family comet 67P/C-G, which has regional-scale strength of tens of Pa based on cliff heights [4], and a surface strength >4 MPa based on Philae lander operations [14]. For a presumably refractory body like Phobos, instead of considering surface ice we note that a thin outer layer of powdery regolith may be more coherent than a blocky interior due to intergranular forces [5, 6, 7]. Our calculations, taken alongside surface observations, support the hypothesis that Phobos has a weak interior (rubble pile) overlain by meters of fine regolith, and that the regolith is developing fissures as the global body deforms due to increasing tides. This is consistent with thermal inertia [15] that indicates the surface or Phobos is fine powder to >~0.1-1 m depth.

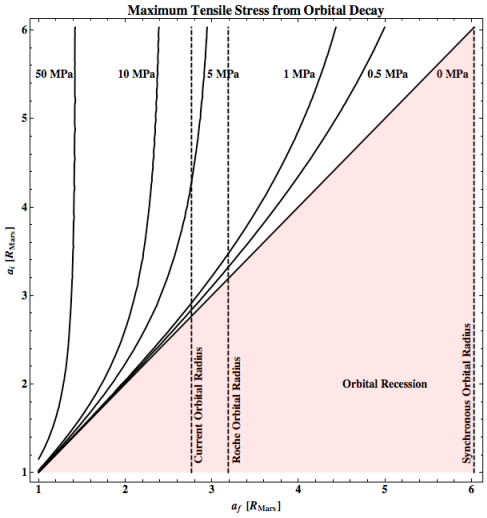

Figure 2. The maximum tensile stress experienced on Phobos for various amounts of orbital decay, from an orbital distance a_i to a_f. Significant stresses could be generated early in Phobos' history, allowing for several generations of surface fractures to evolve.

Discussion

Just because Phobos is fracturing in a thin surface layer does not mean its catastrophic disruption is imminent. A friction angle ~3° is sufficient to prevent downslope movement even in the absence of cohesion [2]. It just means that the interior is weak enough to permit tidal deformation and build up fracture stresses in an outer shell. The deformation computed from Phobos' orbital decay leads to a surface stress field closely aligned with most of the observed grooves. More detailed study by an orbiter or lander will provide better constraints on the satellite's past and near-term geologic evolution, and its suitability for human exploration given what may be an active and evolving surface.

References

[1] Dobrovolskis, A.R. Internal stresses in Phobos and other triaxial bodies. Icarus 52, 136-148 (1982).

[2] Holsapple, K.A. Equilibrium Configurations of Solid Cohesionless Bodies. Icarus 154, 432-448 (2001).

[3] Burns, J.A. The dynamical evolution and origin of the Martian moons. Vista in Astronomy 22, 193-210 (1978).

[4] Sierks et al. On the nucleus structure and activity of comet 67P/Churyumov-Gerasimenko. Science 347 (2015).

[5] Blum, J. Dust Agglomeration, Advances in Physics 55, 881-947 (2006)

[6] Asphaug, E. Growth and Evolution of Asteroids. Annual Review of Earth and Plansetary Sciences 37, 413-448 (2009).

[7] Scheeres, D.J., Hartzell, C.M., Sanchez, P., & Swift, M. Scaling forces to asteroid surfaces: The role of cohesion. Icarus 210, 968-984. (2010).

[8] Soter, S. & Harris, A. Are striations on Phobos evidence for tidal stress? Nature 268, 421-422 (1977).

[9] Sabadini, R. & Vermeersen, B. Global Dynamics of the Earth. Kluwer Academic Publishers, Netherlands (2004).

[10] Kattenhorn, S.A. & Hurford, T.A. Tectonics of Europa. Europa, The University of Arizona Press, Tucson (2009).

[11] Melosh, H.J. Global tectonics of a despun planet. Icarus 31, 221-243 (1977).

[12] Weidenschilling, S.J. A possible origin for the grooves of Phobos. Nature 282, 697-698 (1979).

[13] Murray, J.B. & Heggie, D.C. Character and origin of Phobos' grooves. Planetary and Space Science 102, 119-143 (2014).

[14] Spohn, T. et al. MUPUS – A Thermal and Mechanical Properties Probe for the Rosetta Lander Philae Space Sci. Rev., 128, 1-4, 339-362 (2007)

[15] Lunine J.I., Neugebauer, G., & Jakosky, B.M. Infrared observations of Phobos and Deimos from Viking. Journal of Geophysical Research 87, 10297-10305 (1982).

EPSC Abstracts
Vol. 10, EPSC2015-843, 2015
European Planetary Science Congress 2015

Physical characterization of fast rotator NEOs

J.B. Kikwaya Eluo (1), C.W. Hergenrother (2)
(1) Vatican Observatory, Vatican City, (2) Lunar and Planetary Laboratory, Tucson, Arizona 85721, USA

Abstract

NEOs cannot only be studied dynamically to address their impact hazard, but also physically to undestand various properties important to constrain models of their potential hazard, and also to know what they can tell us about the origin of the solar system and its ongoing processes. But this can only efficiently be done if NEOs are observed with different instruments to cover as much as possible a large portion of the electromagnetic spectrum. Therefore setting up a network of telescopes to observe simultaneously Near-Earth Objects with different instruments in different bands will provide complemetary properties that will help to understand them.

1. Introduction

Our project is to take advantage of the two-meter-class telescopes around Tucson, in Arizona in USA to observe fast rotator NEOs (H $>$ 22) synoptically at three different locations: VATT (Vatican Advanced Technology Telescope) at Mount Graham (longitude: -109.8719, latitude: 32.7016, elevation: 10469 feet), Bok 2.3 m at Kitt Peak (longitude: -111.6004, latitude: 31.9629, elevation: 6795 feet) and Kuiper 1.5-m at Mount Bigelow (longitude: -110.7345, latitude: 32.4165, elevation: 8235 feet). All three telescopes will aim simultaneously at the same object, each with a different instrument. Since 2013, The VATT-4K, optical imager mounted on the VATT, is used for photometry. In the future we plan to utilize the BCSpec (Boller & Chivens Spectrograph) for visible spectroscopy on Bok 2.3 meter and a near-infrared instrument on Kuiper 1.5 meter.

2 Instrument and data

VATT (Vatican Advanced Technology Telescope) is a telescope operated by the Vatican Observatory. It has 1.8-m f/1.0 primary mirror, and 0.38-m f/0.9 Zerodur concave secondary mirror. VATT4k, an imager, is mounted on the VATT for photometry and astrometry. It has a field of view of 12.5 arcmin square with a scale of 0.375"/pixel. The resolution of images acquired with this instrument have a resolution of 2016x2016 pixels, covering 300 to 1000 nm with a quantum efficiency of 96% at 450 nm. Broadband BVRI filters are used for color estimation of NEOs. Data gathered are from April 2013 to March 2015.

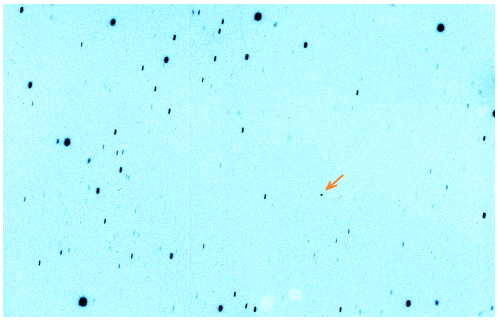

Figure 1: NEO 2011PT.

3 Reduction and Analysis

Iraf commands like ccdphot, digiphot, apphot are used to perform photometry reduction. Radii of the sky annulus are fixed. Imexam is used to estimate the object radius for each frame and twice the value is inserted as the object aperture. 3 BVRI photometric standard stars are used each night [1] at different magnitude and different airmass. For each standard star, total magnitude is given by catalog magnitude - Instrumental magnitude. Linear fit of total magnitude versus airmass gives zero point (intercept) and slope (extinction coefficient). Object magnitude on one frame is given by (zero point magnitude + Instrumental magnitude) - object air mass* extinction coeeficient. Asteroid Lightcurve Analysis program by Petr Pravec is used to estimate the rotation of the object [2] and also the color indexes B-V, V-R and I-R. Some NEOs with

their different spinning rates are shown below.

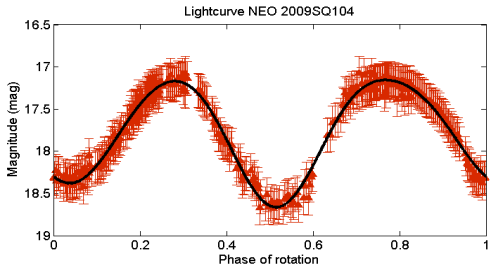

Figure 2: 2009 SQ104 (6.85 $\pm$ 0.03 h).

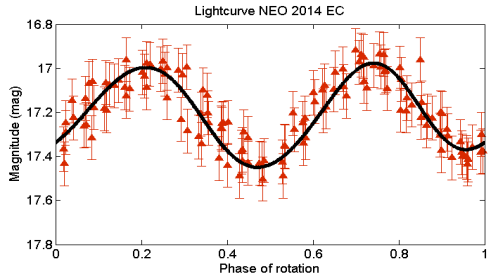

Figure 3: 2014 EC (0.54 $\pm$ 0.04 h).

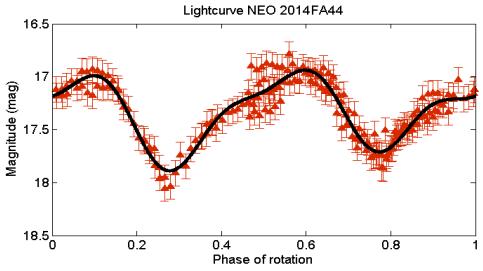

Figure 4: 2014 FA44 (3.45 $\pm$ 0.05 h).

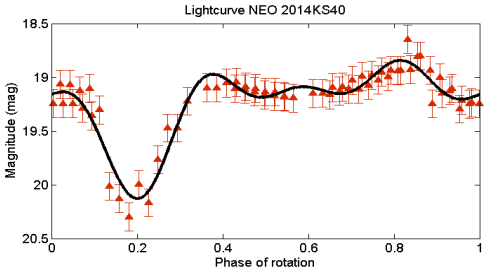

Figure 5: 2014 KS40 (1.11 $\pm$ 0.06 h).

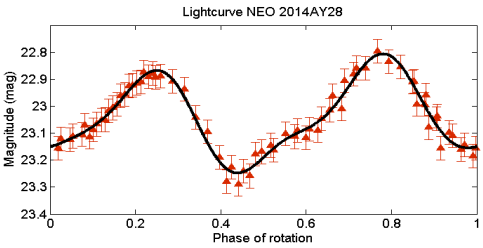

Figure 6: 2014 AY28 (0.91 $\pm$ 0.02 h).

4 Results and Conclusions

2009 SQ 4109, 2014 EC, 2014 FA44, 2014 KS40, 2014 SB145, 2014 AY28, 2011 PT, 2014 SC324, and 2014 WF201 showed clear spinning rate, but 2014 HM2 did not show any conclusive spinning rate. Using Figure 5 of F. Yoshida et al (2004) [3], seven objects are associated to different NEO groups. 2014 HM2, 2014 FA, 2014 SB145, 2011 PT fall among X-type asteroids; 2014 KS40, 2014 WF201 are likely to be C-type; and 2014 SC 324 is a D-type.

References

[1] LANDOLT, 1992, AJ, 104, 340

[2] Petr PRAVEC, Asteroid Lightcurve Analysis Program (Version 0.94.3)

[3] F. YOSHIDA, 2004, PASJ, 56, 1105

EPSC Abstracts
Vol. 10, EPSC2015-887-2, 2015
European Planetary Science Congress 2015

Modelling of the YORP effect

O. Golubov (1,2)
(1) V. N. Karazin Kharkiv National University, Kharkiv, Ukraine, (2) Institute of Astronomy of V. N. Karazin Kharkiv National University, Kharkiv, Ukraine (olexiy.golubov@gmail.com)

Abstract

In the talk I will review the recent advances in the theoretical understanding of the YORP effect. I describe the standard mathematical formalism used for the YORP effect, with the special focus on the limitations of the standard theory and its possible genaralizations. I discuss the sensitivity of the YORP effect to small-scale structures and the novel concept of the tangential YORP, a torque that alters even the rotation of symmetric asteroids due to uneven heat conductivity in small stones composing the surface. Finally, I consider the overall evolution of an asteroid experiencing the YORP effect.

1. Introduction

The Yarkovsky–O'Keefe–Radzievskii–Paddack (or YORP) effect was first proposed by Rubincam in 2000 as recoil torque produced by light emitted or scattered by an asteroid [6]. Since then it established itself as a primary driving force causing evolution of rotation states of small asteroids, acquired many observational confirmations and a sophisticated theoretical description[9].

2. Normal YORP effect

The YORP effect of a convex asteroid with no thermal inertia can be expressed as a surface integral of a function depending on the properly averaged illumination [8].

Equations from [8] deduced for convex asteroids appear to provide a descent approximation for moderately concave shapes. This approach can also be generalized for the case of non-zero thermal inertia [4]. The genaralization is significant only for the obliquity component of the effect, while the axial component of YORP under very broad conditions does not depend on the thermal model. Considering elliptical orbits and scattering laws other then Lambert's present additional amendments of the YORP theory [4].

3. Sensitivity of YORP to small scale structure

Most approachas to the normal YORP rely on local flatness of the surface. But the YORP effect is sensitive to roughness of the surface on the small scale [7]. Asteroid (25143) Itokawa is an especially interesting case, as a high resolution shape model is available for it, but still theoretical predictions for the magnitude of the YORP acceleration differ greatly not only from the observed acceleration, but even with each other [3]. Decomposing the shape of the asteroid into spherical harmonics allows to estimate the error in the YORP acceleration (see the talk by U. Pyrohova).

4. Tangential YORP

Tangential YORP (or TYORP) presents another alteration of the notion of YORP originating from non-flatness of the surface. TYORP appears due to uncompensated heat fluxes through small stones on the surface of an asteroid, causing preferrential emission of infrared radiation eastward rather than westward, and a recoil pressure spinning up the asteroid. TYORP always acts in concert with the normal YORP (or NYORP), and although TYORP force is about two orders of magnitude less than NYORP force, the two torques can be comparable, as NYORP torques of different parts of the surface tend to subtract, while TYORP torques tend to add up. The effect was initially simulated in one-dimentional model [2], then with three-dimentional spherical stones [3], but simulations in more realistic models are still necessary.

5. Overal evolution of rotation state

Distribution of small asteroids over rotation rates and obliquities is formed predominantly by the YORP torques, which continiously alter the angular momentum of the asteroid [5].

If in the course of this alteration an asteroid acquires too big angular momentum, centrifugal forces acting

on the surface can make the shape of the asteroid unstable. Then landslides will start changing the shape, which will also influence the YORP acceleration and possibli stop the further increase in the rotation rate. If it does not happen, the asteroid can increase its rotation so much, that matter starts escaping its surface. The escaping matter can form a satellite, which will eventually leave the primary asteroid, carying a substantial fraction of the angular momentum.

6. Unanswered questions

Still, many important questions remain unanswered.

1. *Global evolution of rotation state.* The question of how the YORP torques translate into global evolution of rotation state has been addressed only in a simplified one-dimensional model with no consideration of the obliquity change [5], while the coupled evolution of obliquity could substancially change the results.

2. *Sensitivity to small-scale structure.* YORP is known to be sensitive to small-scale structure of the surface [7], but a more elaborate error estimate for real shape models of asteroids is necessary. Moreover, Itokawa paradox still persists [3].

3. *Disruption of fast rotators.* For fast rotators, the mechanics of landslides, disruption, and satellite formation are still poorly understood.

4. *Tumbling.* For slow rotators, there is still no self-consistent description of tumbling, including the YORP torque and inelastic energy dissipation.

Acknowledgements

I am very grateful to my teachers Dr. Yu. N. Krugly and Prof. D. J. Scheeres, and to my students U. Pyrogova and V. Lipatova, in association with whom much of my research in this area was done. I also acknowledge support from NASA Grant NNX11AP24G.

References

[1] Čapek D., Vokrouhlický D. 2004, Icarus, 172, 526

[2] Golubov O., Krugly Yu. N. 2012, ApJL, 752, 11

[3] Golubov O., Scheeres D. J., Krugly Y. N. 2014, ApJ, 794, 22

[4] Golubov O., Kravets Y., Krugly Y. N., Scheeres D. J. MNRAS, submitted

[5] Pravec P., Harris A. W., Vokrouhlický D., et al. 2008, Icarus, 197, 497

[6] Rubincam D. P. 2000, Icarus, 148, 2

[7] Statler T. S., 2009, Icarus, 202, 502

[8] Steinberg E., Sari R. 2011, AJ, 141, 55

[9] Vokrouhlický D., Bottke W. F., Chesley S. R., Scheeres D. J. Statler T. S., 2015, [arXiv:1502.01249]

EPSC Abstracts
Vol. 10, EPSC2015-895-2, 2015
European Planetary Science Congress 2015

Sensitivity of the YORP effect to small perturbations of the asteroid shape

U. Pyrohova (1), O. Golubov (1,2)
(1) Institute of Astronomy of Kharkiv National University, 35 Sumska Str., Kharkiv, 61022, Ukraine (ulyana487@gmail.com),
(2) V. N. Karazin Kharkiv National University, 4 Svobody Sq. 4, 61022, Kharkiv, Ukraine

Abstract

We study YORP for an asteroid modelled as a triaxial ellipsoids slightly perturbed by spherical harmonics. The analyticaly obtain the YORP torque as a series in terms of spherical function coefficients. Then we analyze sherical fuction and determine, which spherical functions give vanishing contributions due to symmetries. We find that the largest contribution to the YORP effect is provided by harmonic Y_{42}. We developed a program computing YORP torque for several specific asteroids, whose shapes are determined observationally. Results of the program are used to estimate the error in the YORP effect, produced by neglecting small-scale structures.

1. Introduction

The reemitted lite from the assymetric asteroid surface recoil pressure which could produce the asteroid rotation. As it was shown by [1] that torque can be caused by external geometry of the body. The body must have a certain amount of "windmill" asymmetry. Thus the discribed effect was named as windmill effect. It is not difficult to recignize that figures of revolution or even triaxial ellipsoids wouldn't be spun up.

Yarkovsky, O'Keefe, Radzievskii and Paddack developed paradigm of non-gravitational forces acting on asteroids [3]. And the mechanism for changing the spin state of asteroids is colled Yarkovsky–O'Keefe–Radzievskii–Paddack effect (YORP effect for short). It is significant for kilometer- and smaller-sized asteroids, especially in the near-Earth region.

As the torque depends on asteroid shape it is interesting to research the sensitivity of torques to different scales of shape irragularity [2].

2 YORP of perturbed triaxial ellipsoids

In order to explore dependence of the YORP torque of an asteroid on different scales of shape irregularity we research a specific asteroid model. Persume asteroid as a sphere perturbed by spherical harmonics and stretched along three mutually orthogonal axes. The obtained spheroidal issue is close to a triaxial ellipsoid. Consider the problem of analytical calculation of the YORP effect for it. Fortunaly total YORP effect turns in linearly series of YORP torques of spherical functions.

$$T_z = \sum_{l,m} \tau_{lm} a_{lm} \qquad (1)$$

, here τ_{lm} – YORP torques of spherical functions (or YORP coefficients), a_{lm} –coeffients of decomposition. From the sherical fuction analyze it is not difficult to recognize multiplicity of harmonics which give vanishing contributions due to symmetries. It was found that the largest contribution to the YORP effect is provided by harmonic Y_{42}. Found stong dependence of YORP torque on asteroid elongation.

3 Decomposition of observed shape models into spherical harmonics

We take existing shape models of asteroids obtained either via lightcorve inversion method, or from radar observations, or from direct in situ observations by spacecraft. We fit a triaxial ellipsoid to each shape model, and decompose the residual into spherical harmonics, finding coefficients a_{lm}. The coefficients of the decomposition are assumed to be Gaussian random variables, whose power spectrum is determined via averaging of coefficients of several spherical harmonics.

Then each asteroid appears to be just one single realization of an ansamble of asteroids with the same power spectrum.

For small l the observationally determined power spectrum is very uncertain, because here no meaningful averaging procedure can be applied. For big l the power appears to bee very small, because small features on the asteroid remain unresolved in the shape model. Still, a power-law extrapolation can be done to this area.

4 Sensitivity of YORP to unresolved features

We substitute the power spectrum of a_{lm} determined in Section 3 and YORP coeffients τ_{lm} determined in Section 2 into Eq. 1. To estimate the error in Eq. 1 due to unresolved features of the surface, we must quadratically add errors due all terms beyond resolution of the shape model. In each of these terms the YORP coeffient τ_{lm} is taken from Section 2, and the variance of a_{lm} is taken from the power spectrum.

The obtained results depend on the validity of extrapolations of the power spectrum to big l. But filtering out high harmonics and calculating the YORP for a smoothed model of an asteroid allows us to make a more rigorous error estimate of the YORP effect.

References

[1] Rubincam D. P., 2000, Icarus, 148, 2

[2] Statler T. S., 2009, Icarus, 202, 502

[3] Vokrouhlicky D., Bottke W. F., Chesley S. R., Scheeres D. J., & Statler T. S., 2015, [arXiv:1502.01249]

EPSC Abstracts
Vol. 10, EPSC2015-922, 2015
European Planetary Science Congress 2015

Complex correspondence between families and collisions

A. Milani (1), Z. Knežević (2) and F. Spoto (1,3)
(1) Department of Mathematics, University of Pisa, Italy, (2) Academy of Science, Serbia, (3) SpaceDyS srl, Cascina, Italy
(milani@dm.unipi.it)

Abstract

Asteroid families are identified as statistically significant concentrations of asteroids in the space of proper elements. The purpose of family classifications is meant to be the identification of the largest collisional events occurred during the history of the asteroid main belt. However, are the families as found in 1-1 correspondence with ancient collisional events?

A recent analysis of larger classifications, based on larger and more accurate datasets of proper elements, indicates that this is not the case. There are multiple cratering events on the same parent body. There are collisional families split into two by the YORP effect. There are subfamilies arising from secondary collisions after the one forming a larger family, and this is not limited to recent events. There are families overlapping in proper elements space but with composition incompatible with a common parent body. There are cases not yet understood, but pointing to a complex collisional history.

In total at least 10 cases of complex correpondence between families and collisional events have been identified, more are suspected but not yet supported by enough evidence. Finally, some information can be obtained even from the absence of a family, as in the case of Ceres. The disentagling of these complex collisional histories is an essential step towards the understanding of the asteroid collisional evolution.

EPSC Abstracts
Vol. 10, EPSC2015-923, 2015
European Planetary Science Congress 2015

Surface processes on the asteroid deduced from the external 3D shapes and surface features of Itokawa particles.

A. Tsuchiyama (1) and T. Matsumoto (2)
(1) Kyoto University, Japan, (2) ISAS/JAXA, Japan (atsuchi@kueps.kyoto-u.ac.jp / Fax: +81-75-753-4189)

Abstract

1. Introduction

Particles on the surface of S-type Asteroid 25143 Itokawa were successfully recovered by the Hayabusa mission of JAXA (e.g., [1,2]). They are not only the first samples recovered from an asteroid, but also the second extraterrestrial regolith to have been sampled, the first being the Moon by Apollo and Luna missions. The analysis of tiny sample particles (20-200 μm) shows that the Itokawa surface material is consistent with LL chondrites suffered by space weathering as expected and brought an end to the origin of meteorites (e.g., [2-4]). In addition, the examination of Itokawa particles allow studies of surface processes on the asteroid because regolith particles can be regarded as an interface with the space environment, where the impacts of small objects and irradiation by the solar wind and galactic cosmic rays should have been recorded.

External 3D shapes and surface features of Itokawa regolith particles were examined. Two kinds of surface modification, formation of space-weathering rims mainly by solar wind implantation and surface abrasion by grain migration, were recognized. Spectral change of the asteroid proceeded by formation of space-weathering rims and refreshment of the regolith surfaces.

External 3D shapes and surface morphologies of the regolith particles can provide information about formation and evolution history of regolith particles in relation to asteroidal surface processes. 3D shapes of Itokawa regolith particles were obtained using microtomography [3]. The surface nano-miromorpholgy of Itokawa particles were also observed using FE-SEM [5]. However, the number of particles was limited and genial feature on the surface morphology has not been understood. In this study, the surface morphology of Itokawa regolith particles was systematically investigated together with their 3D structures.

2. Experiments

Eleven and nine particles picked up from Rooms-A and –B of the sample catcher, respectively. They were examined by analytical dual-energy microtomography [6] with the voxel size of about 100 nm at BL47XU of SPring-8 for 3D structures and by FE-SEM (JEOL JSM-7001F, JSM-7800F, Hitachi S-5500, SU-8220) for micro-nanaomorphology. In the SEM observation, the samples were not coated with any conducting materials to avoid possible decoration by the coating. To avoid charge up by electron irradiation, observation was made at a low accelerating voltage (1 or 2 kV) in vacuum.

After the tomography and SEM observation, ultra-thin sections were prepared using focused ion beam (FIB: FEI Quanta 200 3DS FIB) from one of the particles (RB-QD04-0043) for TEM/EDX analysis (JEM-2100F). A high-angle annular dark-field (HAADF) imaging in STEM mode was performed to observe distribution of materials with heavy elements in the sample.

3. Results and Discussions

Based on the SEM observation, the regolith surfaces can be classified into three-types. Type 1 surfaces are represented by nearly parallel and sometimes branched steps. They are regarded as fractured or cleaved surfaces by comparing with fractured and cleaved surfaces of terrestrial olivine and pyroxene grains. These surfaces were formed by impact on the

Itokawa surface. Type 2 surfaces are represented by parallel and/or concentric steps with polygonal shapes. Type 3 surfaces are covered with many micron-submicron mineral grains, which are connected to the substrates based on the CT observation. These grains usually have facets and show euhedral shapes. Type-2 and -3 surfaces resemble to products in vapor condensation experiments of olivine [7], and thus can be regarded as condensates from vapor. Particles having these surface types are porous in the CT images. They should be walls of closed cavities or "micro-druses", which were formed from originally porous aggregates of fine materials such as matrix or fine regolith breccia at high temperatures during thermal metamorphism or post-shock heating.

The surfaces can be also categorized into two different types; fresh surfaces having sharp edges, and matured surfaces having rounded edges. They are consistent with the external 3D shapes observed by the microtomography. The fresh and matured surfaces were observed regardless of Types 1-3. A single grain sometimes has the both surface types. The matured surfaces were considered to form from fresh surfaces by abrasion processes on Itokawa [3].

Blister structures were formed by solar wind implantation as a part of space-weathering rims [8]. The SEM and TEM studies of the same location of the same particle showed that blister structures, which were originally observed by TEM [8], were recognized as spotted structures on the particles surfaces by SEM. Eleven out of twenty regolith particles have space-weathered rims with blisters. These rims are heterogeneously distributed in a single particle and the rims often present in opposite surfaces of the same particle, suggesting migration of regolith particles on Itokawa. In addition, the blister distribution and the roundness of the particle surface are not correlated with each other. Thus, the abrasion process can be regarded as a different type of space weathering with a longer timescale, and should be called "space micro-erosion." The abrasion is probably the result of grain migration, which is caused by seismic waves repeatedly reflecting off the surface of Itokawa after impacts [3]. Different potential mechanisms for the physical weathering, tidal disruption and YORP effect, was also proposed [9].

The present results indicate that space-weathering process of Asteroid Itokawa proceeded as follows. Space-weathered rims were developed on local surfaces of individual regolith particles, promoting the spectral change of Asteroid Itokawa, while refreshment of the regolith surfaces occurred, suppressing the spectral change, by mechanical abrasion due to grain migration and fragmentation due to impact.

Acknowledgements

The authors are grateful to Preliminary Examination team members and the Hayabusa project.

References

[1] Nakamura T and 21 authors: Itokawa dust particles: A direct link between S-type asteroids and ordinary chondrites. Science 333, 1113-1116, 2011.

[2] Tsuchiyama A.: Asteroid Itokawa. A source of ordinary chondrites and a laboratory for surface processes. Elements, 10, 45-, 2014.

[3] Tsuchiyama A and 32 coauthors: Three-dimensional structure of Hayabusa samples: Origin and evolution of Itokawa regolith. Science 333, 1125-1128, 2011.

[4] Noguchi T. and 17 coauthors: Incipient space weathering observed on the surface of Itokawa dust particles. Science, 333, 1121-1125, 2011.

[5] Nakamura E. and 17 coauthors: Space environment of an asteroid preserved on micrograins returned by the Hayabusa spacecraft. Proceedings of the National Academy of Sciences, 109, E624-E629, 2012.

[6] Tsuchiyama A. and 12 coauthors: Analytical dual-energy microtomography: A new method for obtaining three-dimensional mineral phase images and its application to Hayabusa samples. Geochimica et Cosmochimica Acta, 116, 5-16, 2013.

[7] Kobatake H. and 5 coauthors: Crystallization of cosmic dust from highly supersaturated silicate vapor in a rapidly cooled environment. *Icarus* 198, 208–217, 2008.

[8] Noguchi T. and 23 coauthors: Space weathered rims found on the surfaces of the Itokawa dust particles. Meteoritics & Planetary Science. 49, 188-214, 2014.

[9] Connolly Jr. H. C., Lauretta, Walsh K. J., Tachibana S., and Bottke W. F.: The dynamical evolution of Asteroid 25143 Itokawa: constraints from sample analysis. Meteoritics & Planetary Science, 49: supplement, A78, 2014.